

Discovery of 3-Hydroxy-3-phenacyloxindole Analogues of Isatin as Potential Monoamine Oxidase Inhibitors

Rati K. P. Tripathi,^[a] Sairam Krishnamurthy,^[b] and Senthil R. Ayyannan^{*[a]}

A series of 3-hydroxy-3-phenacyloxindole analogues of isatin were designed, synthesized, and evaluated in vitro for their inhibitory activity toward monoamine oxidase (MAO) A and B. Most of the synthesized compounds proved to be potent and selective inhibitors of MAO-A rather than MAO-B. 1-Benzyl-3-hydroxy-3-(4'-hydroxyphenacyl)oxindole (compound **18**) showed the highest MAO-A inhibitory activity (IC_{50} : $0.009 \pm 0.001 \mu\text{M}$, K_i : $3.69 \pm 0.003 \text{ nM}$) and good selectivity (selectivity index: 60.44). Kinetic studies revealed that compounds **18** and **16** (1-benzyl-3-hydroxy-3-(4'-bromophenacyl)oxindole) exhibit competitive inhibition against MAO-A and MAO-B, respectively.

Structure–activity relationship studies suggested that the 3-hydroxy group is an essential feature for these analogues to exhibit potent MAO-A inhibitory activity. Computational studies revealed the possible molecular interactions between the inhibitors and MAO isozymes. The computational data obtained are congruent with experimental results. Further studies on the lead inhibitors, including co-crystallization of inhibitor–MAO complexes and in vivo evaluations, are essential for their development as potential therapeutic agents for the treatment of MAO-associated neurological disorders.

Introduction

Monoamine oxidases (MAOs, amine-oxygen oxidoreductase, EC 1.4.3.4) are flavin adenine dinucleotide (FAD)-containing enzymes bound to the outer mitochondrial membrane of neuronal, glial, and other cells.^[1,2] These enzymes are responsible for the oxidative deamination of neurotransmitters and other dietary amines.^[3,4] Two isoforms of MAO have been identified, MAO-A and MAO-B, based on their primary sequences, 3D structures, substrate sensitivity, and inhibitor selectivity.^[5–8] MAO-A has a higher affinity for serotonin and norepinephrine, whereas MAO-B preferentially catalyzes the deamination of β -phenylethylamine.^[9] These properties determine the clinical interest of MAO inhibitors (MAOIs). Selective MAO-A inhibitors, such as clorgyline and moclobemide are used for the treatment of depression and anxiety,^[10,11] whereas selective MAO-B inhibitors, such as selegiline and rasagiline, are useful as adjuvants for the treatment of Parkinson's^[12,13] and Alzheimer's diseases.^[14,15] Because of the poor efficacy of the currently available drugs, an intensive search for new and innovative MAOIs is still needed. Efforts toward the discovery of ideal drug candidates for the treatment of neurological disorders have increased considerably in recent years.^[16–20]

Isatin (2,3-dioxindole) has been documented as a well-known pharmacological agent that possesses a broad range of actions in biological systems. Isatin has also been identified as a major component of tribulin, a family of naturally occurring low-molecular-weight non-peptide inhibitors of MAO.^[21] This endogenous compound has been reported as a moderately potent inhibitor of human MAO-B, with an enzyme–inhibitor dissociation constant (K_i value) of $3 \mu\text{M}$. It also inhibits human MAO-A with a K_i value of $15 \mu\text{M}$.^[22] Isatin and its natural and synthetic derivatives display diverse pharmacological activities. The isatin scaffold also appears as a component of many synthetic compounds that exhibit a wide range of effects^[23,24] including anticonvulsant, anxiolytic, antitubercular, and antitumor activities.

Compounds with the isatin moiety have been well documented as promising scaffolds for the development of new therapeutic agents for the treatment of central nervous system disorders. 3-Hydroxy-3-substituted oxindoles derived from isatin were reported to possess anticonvulsant activity with no or minimal toxicity. Within the context of enzyme inhibitors, isatins have seen applications in the inhibition of monoamine oxidases. Several isatin derivatives were found to possess both MAO-A and MAO-B inhibitory properties with very low or no neurotoxicity.^[25–27] Figure 1 illustrates a few examples of isatin derivatives (**1** and **2**) that possess good activity against MAO, and few reference MAO inhibitors (compounds **3–6**).^[28–32]

Isatin is therefore a biologically validated starting point for the design of chemical libraries directed at targeting the MAO isozymes.^[22,23] Due to the privileged nature of isatin, it can be predicted that chemical libraries of this scaffold should yield medicinally active compounds with high hit rates.

[a] R. K. P. Tripathi, Dr. S. R. Ayyannan
Pharmaceutical Chemistry Research Laboratory
Department of Pharmaceutics, Indian Institute of Technology
Banaras Hindu University, Varanasi 221005, Uttar Pradesh (India)
E-mail: asraja.phe@iitbhu.ac.in

[b] Dr. S. Krishnamurthy
Neurotherapeutics Laboratory
Department of Pharmaceutics, Indian Institute of Technology
Banaras Hindu University, Varanasi 221005, Uttar Pradesh (India)

 ORCID(s) from the author(s) for this article is/are available on the WWW under <http://dx.doi.org/10.1002/cmdc.201500443>.

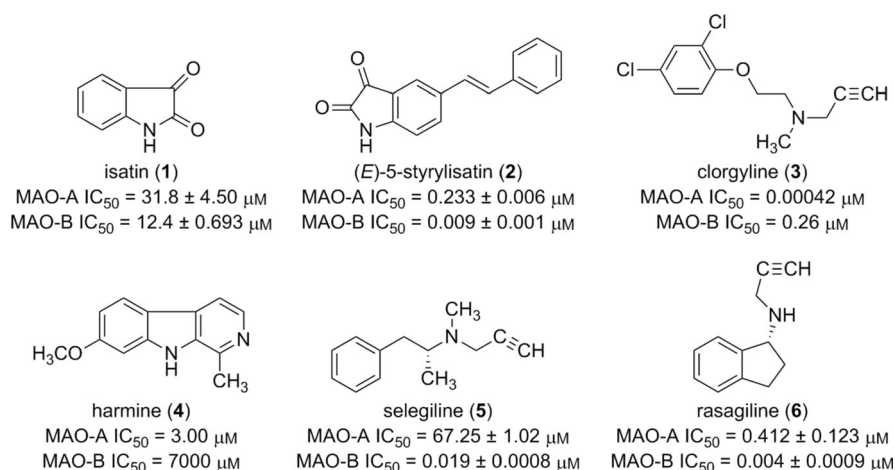


Figure 1. MAO inhibitory activity of a few isatin derivatives and reference inhibitors.

The solution of crystal structures of MAO enzymes alone and in complex with their respective inhibitors has significantly enhanced the rate of identification of new potent inhibitors. The high-resolution three-dimensional (3D) structure of a complex between isatin and human recombinant MAO-B shows that isatin binds within the substrate cavity in close proximity to the FAD co-factor with the dioxindolyl NH group and the C2 carbonyl oxygen atom hydrogen bonded to conserved water molecules within the active site. This binding mode leaves the entrance cavity of MAO-B unoccupied (Figure 2).^[8]

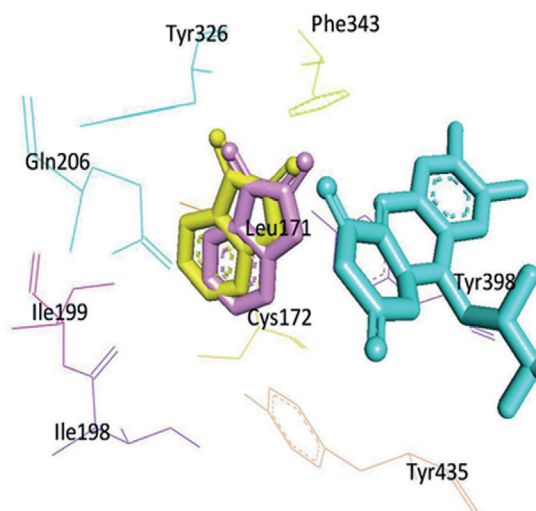


Figure 2. AutoDock-generated pose of isatin with gold-standard pose (GSP) of isatin (PDB ID: 1OJA) in the MAO-B active site. Selected residues are depicted in black. Isatin, GSP of isatin, and FAD are shown in pink, yellow, and cyan, respectively.

A high-resolution 3D structure of isatin bound to MAO-A has not yet been determined. However, a lower-resolution structure of MAO-A was determined in order to understand the catalytic and inhibitory mechanisms. Ma et al.^[5] first determined the X-ray crystal structure of rat MAO-A at 3.2 Å resolution, and later the structure of human MAO-A was solved by De Co-

libus et al.^[6] at a resolution of 3.0 Å. In 2008, Son et al. reported the X-ray crystal structure of human MAO-A co-crystallized with a potent MAO-A-specific inhibitor, harmine, at 2.2 Å resolution.^[7] Harmine, a β-carboline alkaloid found in plants,^[33] selectively binds to MAO-A, but does not inhibit the variant MAO-B.^[34] The high-resolution structure of harmine in complex with MAO-A has provided greater insight into the enzymatic properties and substrate/inhibitor binding specificities of MAO-A. Harmine is found to be located in the active site cavity of the enzyme and interacts with several residues: Tyr69, Asn181, Phe208, Val210, Gln215, Cys323, Ile325, Ile335, Phe352, Tyr407, Tyr444, and FAD.

With a view to identify novel heterocyclic compounds as potent MAO inhibitors that could serve as potential chemical templates for drug discovery, we designed a series of 3-hydroxy-3-phenacyloxindoles by incorporating a benzyl moiety at the 1-position and/or a bromo group at position 5, and (un)-substituted phenacyl group at position 3. The design approach is depicted in Figure 3. It is presumed that the versatile isatin

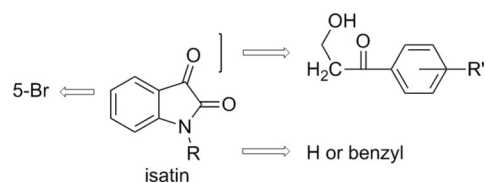


Figure 3. Structural modifications to the isatin scaffold.

moiety, being a rigid stable electron-rich region, can serve as a hydrophobic and/or hydrogen bonding site while the 3-phenacyl-substituted systems can offer hydrophobic interactions with the active site of MAO.

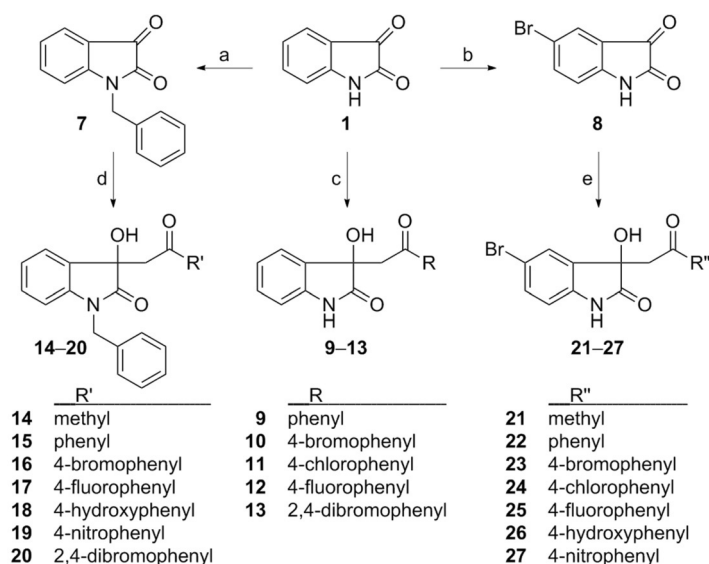
The present work includes the synthesis, in vitro and in silico MAO-A and MAO-B inhibition studies of 3-hydroxy-3-phenacyloxindoles (compounds 9–27) derived from isatin and comparison of their MAO-A and MAO-B binding and inhibitory potentials with those of the reference inhibitors. Kinetic studies were carried out to examine the modes of inhibition of the most

active inhibitors (compounds **18** and **16**) against MAO-A and MAO-B, respectively. Furthermore, computational evaluations of MAO-A and MAO-B inhibitors by docking simulations (Auto-Dock 4.2) were performed to gain structural insight into the binding modes and possible interactions of the inhibitor compounds within the active sites of MAO-A and MAO-B and also to determine the free energy of binding (ΔG) and inhibition constants (K_i) of the experimentally tested MAO-A and MAO-B inhibitors.

Results and Discussion

Chemistry

The intermediates and final compounds were synthesized according to well-established procedures,^[25–27] but with modifications wherever needed. The synthetic route followed for compounds **7–27** is outlined in Scheme 1. *N*-Benzylisatin **7** and 5-



Scheme 1. Synthesis of 3-hydroxy-3-phenacyloxindole analogues **9–27**. *Reagents and conditions:* a) $C_6H_5CH_2Cl$, DMF, K_2CO_3 , reflux, 4 h; b) Br_2 , $0^\circ C$, glacial acetic acid; c) acetone or substituted acetophenones ($R-COCH_3$), $HN(C_2H_5)_2$, C_2H_5OH , reflux, 30 min; d) $R'-COCH_3$, $HN(C_2H_5)_2$, C_2H_5OH ; e) $R''-COCH_3$, $HN(C_2H_5)_2$, C_2H_5OH , reflux, 30 min.

bromoisatin **8** were obtained by reaction of isatin **1** with benzyl chloride and bromine, respectively.^[35,36] 3-Hydroxy-3-phenacyloxindole analogues of unsubstituted isatin (**9–13**), *N*-benzylisatin (**14–20**), and 5-bromoisatin (**21–27**) were obtained through Knoevenagel condensation of the appropriate isatin with acetone or substituted acetophenones in the presence of diethylamine as basic catalyst. When an ethanolic solution of isatin or substituted isatin and acetone or substituted acetophenone containing a small quantity of diethylamine was held at reflux for 30 min and then allowed to stand for few days, copious yields of product compounds **9–27** were obtained. The products were evidently the result of interaction of reactive β -carbonyl group of isatin or substituted isatin with the methyl group of acetone or substituted acetophenone. The proposed

mechanism of this condensation reaction is depicted in Scheme 2. Details of the physicochemical and spectral characterization of the synthesized compounds are given in Experimental Section below, and are in good agreement with the composition of the synthesized compounds.

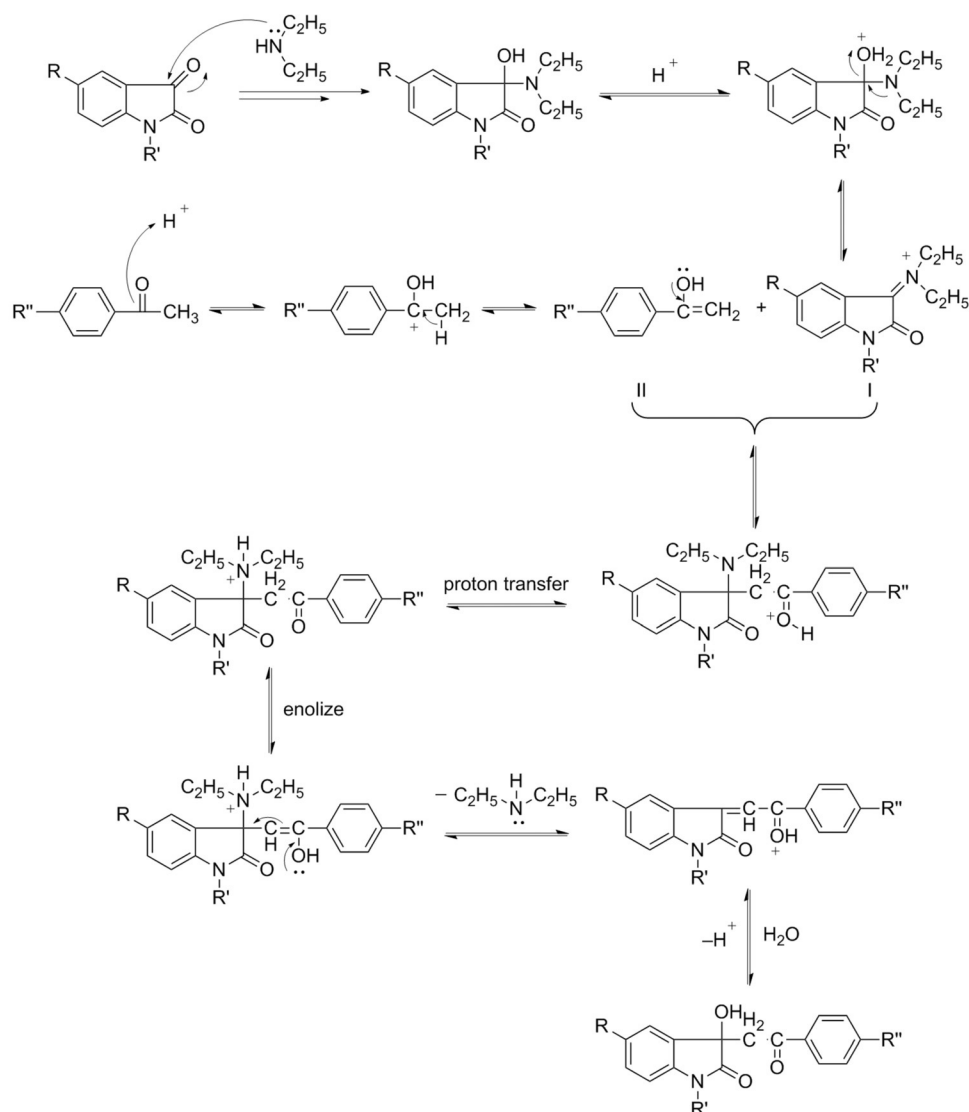
Enzyme inhibition assays

MAO-A and MAO-B inhibitory activities of test compounds **9–27** expressed in terms of IC_{50} values are listed in Table 1. The inhibitory activity of test compounds was measured in vitro by a spectrophotometric method, by using crude rat brain mitochondrial suspensions, as reported. For comparison, the inhibitory potencies of reference inhibitors isatin (**1**), clorgyline (**3**), harmine (**4**), selegiline (**5**), and rasagiline (**6**) are also presented in Table 1.

The test compounds exhibited significant MAO inhibitory activity, with IC_{50} values in the micromolar to sub-micromolar range. The IC_{50} values are in the range of $0.009 \pm 0.001 \mu M$ (compound **18**) to $1.057 \pm 0.019 \mu M$ (compound **9**) for MAO-A, and $0.111 \pm 0.001 \mu M$ (compound **16**) to $5.654 \pm 0.043 \mu M$ (compound **9**) for MAO-B. To gain more insight into the structure–activity relationships (SARs), focused structural modifications were attempted on the isatin scaffold to vary the lipophilic, electronic, and steric properties. In general, all structural variations attempted in the scaffold resulted in improved inhibitory activity. In particular, the enhancement of lipophilicity (compounds **14–20**) by incorporating a benzyl moiety at position N1 and bromoaryl or hydroxyaryl substituents at position 3 of the isatin scaffold resulted in improved inhibitory activity against the MAO isozymes.

1-Benzyl-3-hydroxy-3-(4'-hydroxyphenacyl)oxindole (**18**, IC_{50} : $0.009 \pm 0.001 \mu M$) emerged as the most active inhibitor examined toward MAO-A, followed by 1-benzyl-3-hydroxy-3-(4'-bromophenacyl)oxindole (**16**, IC_{50} : $0.013 \pm 0.001 \mu M$). The most active MAO-B inhibitor, compound **16**, was found to exhibit an IC_{50} value of $0.111 \pm 0.001 \mu M$ followed by 1-benzyl-3-hydroxy-3-phenacyloxindole (**15**, IC_{50} : $0.184 \pm 0.005 \mu M$).

Notably, all compounds displayed mild-to-moderate selectivity for MAO-A over MAO-B (Table 1). Alterations in the electronic and steric features afforded by the presence of various mono- or disubstituted phenyl rings at C3 significantly influenced the MAO inhibitory profile of these compounds. Interestingly, the 4-hydroxy-substituted analogue (compound **18**) was found to be the most potent MAO-A inhibitor among the other analogues with the highest selectivity index of 60.44. This potential activity and selectivity can be attributed to the presence of a 4-hydroxy substituent on the phenacyl side chain. However, bromo (**16** and **20**, 1.5- and 2-fold less potent than **18**) and fluoro (**17**, nearly 11-fold less potent than **18**) substitutions on the phenacyl side chain resulted in decreased inhibitory potency against MAO-A, which may be due to variations in the electronic properties imparted by these groups. Among the 5-bromoisatin analogues (**21–27**),



Scheme 2. Proposed condensation reaction mechanism between isatin and substituted acetophenone.

the chloro-substituted analogue (compound **24**) was found to be the most active, with an IC₅₀ value of 0.071 μM; this compound was found to be almost 8-fold less potent than the lead MAO-A inhibitor, compound **18**.

The inhibitory data indicate that *N*-benzylisatin analogues **14–20** are more active than *N*-unsubstituted isatins **9–13** and 5-bromoisatin analogues **21–27**. Thus, the ranking order of these inhibitors for potency against MAO-A as per experimental inhibitory data is: **18** > **16** > **20** > **15** > **24** > **13** > **17** > **19** > **14** > **22** > **21** > **27** > **10** > **23** > **26** > **25** > **11** > **12** > **9**, whereas the ranking according to computational data is: **18** > **20** > **16** > **15** > **17** > **19** > **22** > **14** > **24** > **13** > **21** > **27** > **10** > **23** > **26** > **25** > **11** > **12** > **9**. Therefore, a good correlation of the *in vitro* and *in silico* data is observed for MAO-A inhibition.

In contrast to its effect on MAO-A inhibitory potency, the presence of a 4-hydroxy group on the phenacyl side chain (compound **18**) did not exhibit a pronounced enhancement in MAO-B inhibitory potency. Compound **16** was found to only

moderately inhibit MAO-B, with an IC₅₀ value of 0.111 μM, ~6-fold less potent than the potency of selegiline.

Thus, substitution with functional groups such as hydroxy, bromo, chloro, and fluoro at the C3 phenacyl ring increased potency toward MAO-A. Among the non-functionalized phenacyl analogues **9**, **15**, and **22**, compound **15**, bearing an *N*-benzyl moiety, was more active (IC₅₀: 0.059 μM), which further supports the above observation claiming the crucial role of the *N*-benzyl group for potent MAO-A inhibitory activity. Moreover, the presence of a bulkier substituent such as a nitro group resulted in less potent analogues (compounds **19** and **27**). These results guide us toward the influence of the steric groups and electronic substituents on the MAO inhibitory profile.

Kinetic studies

To further examine the modes of MAO-A and MAO-B inhibition, sets of Lineweaver–Burk plots were constructed for the inhibition of MAO-A by compound **18** and MAO-B by compound **16**,

Table 1. In vitro and computational MAO inhibition data for compounds 9–27 along with reference inhibitors.

Compd	MAO-A			MAO-B			SI ^[a]
	In vitro IC ₅₀ [μM] ^[b]	In silico ΔG [kcal mol ⁻¹]	In silico K _i [μM]	In vitro IC ₅₀ [μM] ^[b]	In silico ΔG [kcal mol ⁻¹]	In silico K _i [μM]	
9	1.057 ± 0.019	-4.95	235.65	5.654 ± 0.043	-6.21	28.28	5.35
10	0.265 ± 0.003	-6.31	23.51	0.391 ± 0.005	-7.08	6.47	1.48
11	0.738 ± 0.008	-5.63	74.05	0.787 ± 0.013	-6.93	8.26	1.07
12	0.911 ± 0.006	-5.57	82.75	3.615 ± 0.052	-6.6	14.49	3.97
13	0.092 ± 0.002	-6.43	19.41	0.192 ± 0.006	-7.67	2.38	2.09
14	0.128 ± 0.007	-6.5	17.08	0.931 ± 0.016	-6.69	12.57	7.27
15	0.059 ± 0.003	-7.67	2.4	0.184 ± 0.005	-8.02	1.22	3.12
16	0.013 ± 0.001	-8.34	0.77	0.111 ± 0.001	-8.53	0.56	8.54
17	0.102 ± 0.004	-7.39	3.83	0.199 ± 0.008	-7.46	3.4	1.95
18	0.009 ± 0.001	-9.19	0.18	0.544 ± 0.004	-9.1	0.21	60.44
19	0.118 ± 0.001	-6.94	8.15	0.314 ± 0.012	-7.24	4.9	2.66
20	0.018 ± 0.006	-9.08	0.22	0.677 ± 0.002	-8.67	0.44	37.61
21	0.142 ± 0.009	-6.38	21.05	2.799 ± 0.034	-5.95	43.2	19.71
22	0.138 ± 0.005	-6.56	15.59	0.592 ± 0.024	-6.71	11.99	4.29
23	0.301 ± 0.012	-6.14	31.57	0.342 ± 0.008	-7.27	4.69	1.14
24	0.071 ± 0.003	-6.49	17.36	0.235 ± 0.003	-7.33	4.27	3.31
25	0.681 ± 0.007	-5.86	50.62	0.925 ± 0.017	-6.89	8.86	1.36
26	0.591 ± 0.002	-6.06	35.85	1.326 ± 0.029	-6.81	10.18	2.24
27	0.148 ± 0.004	-6.31	23.66	0.513 ± 0.016	-7.04	6.92	3.47
1 ^[28]	31.8 ± 4.50	-	-	12.4 ± 0.693	-4.74	333.71	-
3 ^[29]	0.00042	-	-	0.26	-	-	-
4 ^[30]	3.00	-5.3	130.82	7000	-	-	-
5 ^[31]	67.25 ± 1.02	-	-	0.019 ± 0.0008	-	-	-
6 ^[32]	0.412 ± 0.123	-	-	0.004 ± 0.0009	-6.51	16.8	-

[a] Selectivity index for MAO-A: IC₅₀(MAO-B)/IC₅₀(MAO-A). [b] Test compound concentration required for 50% inhibition of enzyme activity; values are the mean ± SEM; *p* < 0.05 versus the corresponding IC₅₀ values obtained against MAO-A and MAO-B, as determined by ANOVA/Dunnett's.

the respective selected representative MAO-A and MAO-B inhibitors (Figure 4). Analysis of the Lineweaver–Burk plots suggests that compounds **18** and **16** inhibit MAO-A and MAO-B competitively, as the plots are linear and intersect at the y axis.^[28]

Determination of K_i

For each type of mode of inhibition, K_i values can be calculated, reflecting the strength of the interactions between the enzyme and the inhibitor. Inhibition constants for competitive inhibitors were calculated (GraphPad Prism software), resulting in K_i values of 3.69 ± 0.003 nM for compound **18** and 5.6 ± 0.12 nM for compound **16**. In comparing the IC₅₀ values with the K_i values, a 2.5-fold difference was observed for compound **18**, and a 20-fold difference was observed for compound **16**, which reflects tight binding of the inhibitor to the enzyme.

Reversibility and irreversibility experiments

Compound **18**, the most active MAO-A inhibitor, was further subjected to time-dependent inhibition studies to investigate whether the observed enzyme inhibition is reversible or irreversible. The reversibility test was performed by using a slightly modified method described by Legoabe et al.^[37] As shown in Figure 5, there is no time-dependent decrease in the rates of MAO-A-catalyzed oxidation of serotonin if compound **18** was pre-incubated with the enzyme for various periods of time (0,

15, 30, and 60 min). From this result it may be concluded that the inhibition of MAO-A is reversible, at least for the maximum time period assayed (60 min). Interestingly, a marked increase in the MAO-A catalytic rate with increased pre-incubation time with compound **18** was observed.

In silico studies

Computational studies were carried out to shed some light on the peculiar binding modes and interactions of MAO inhibitors with the MAO isozymes in addition to affinity and selectivity. All experimentally tested inhibitors (compounds 9–27) were docked successfully into the catalytic sites of MAO-A and MAO-B using the automated docking program AutoDock 4.2 as per the protocol described.^[38] The best-scoring conformers from the largest cluster were considered for further structural and interaction studies. The results of the docking studies for both MAO-A and MAO-B, expressed in terms of theoretical inhibition constants (K_i values) and estimated binding energies (ΔG) for each virtual enzyme–inhibitor complex, are listed in Table 1.

Pose analysis of MAO-A inhibitors

Visual inspection of binding modes of all inhibitors within the active site of MAO-A and MAO-B was done to gain more insight into the binding orientation and potential inhibitor–enzyme interactions. The inhibitor binding site of MAO-A is

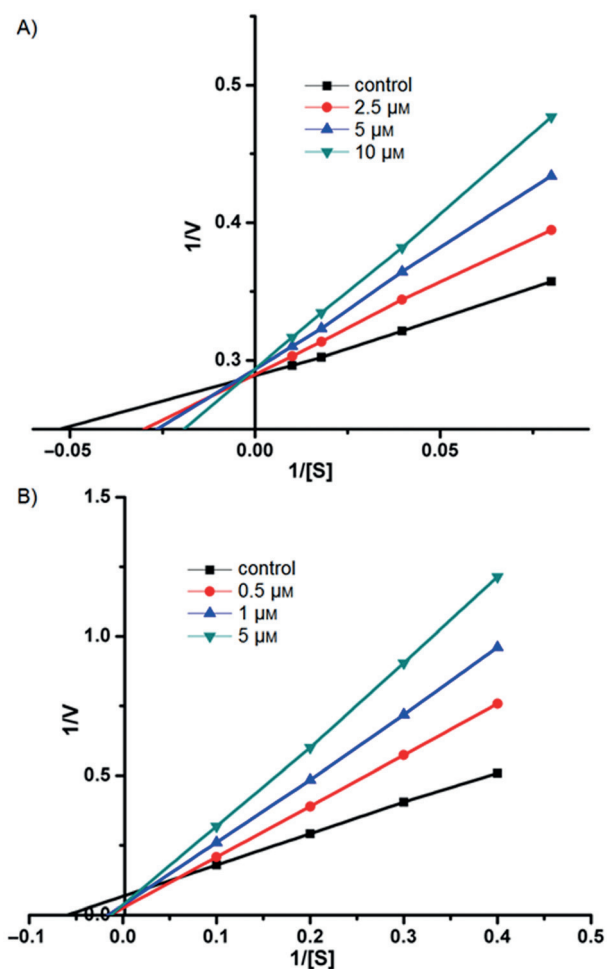


Figure 4. Kinetics of rat brain MAO isozyme inhibition by compounds **18** and **16**: A) Lineweaver–Burk plot of MAO-A-catalyzed oxidation of serotonin in the absence (control) and presence of various concentrations of compound **18** as indicated. B) Lineweaver–Burk plot of MAO-B-catalyzed oxidation of benzylamine in the absence (control) and presence of various concentrations of compound **16** as indicated. Rates (V) are expressed as (nmol product formed) $\text{min}^{-1}(\text{mg protein})^{-1}$.

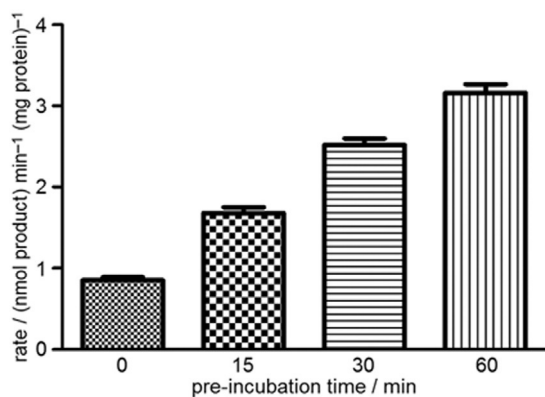


Figure 5. Time-dependent inhibition of MAO-A-catalyzed oxidation of serotonin by compound **18**.

a single cavity that extends from the flavin ring to the cavity-shaping loop. The volume of this cavity is estimated to be

$\sim 500 \text{ \AA}^3$ and is quite hydrophobic.^[6] All inhibitors are located in the active site cavity of MAO-A. Compounds **15**, **17**, and **20** (Figure 6A) and **9–14**, **16**, **18**, **19**, and **21–27** (Figure 6B) share a common binding mode within the MAO-A active site.

Further investigation of the interactions of all inhibitors **9–27** with the anchoring residues present in the MAO-A active site led to the following observations: The potential binding site of these inhibitors was found to be surrounded by the residues Tyr69, Ile180, Asn181, Phe208, Val210, Gln215, Cys323, Ile325, Ile335, Met350, Phe352, Tyr407, Tyr444, and FAD (Figure 6) which is very similar to the binding site environment of the reference MAO-A inhibitor, harmine. In nearly all compounds, the oxindole moiety occupies the center of the cavity with the substituted phenacyl group occupying the cavity extending toward FAD, while the *N*-benzyl group is situated toward the opening of the cavity. At the bottom of the cavity, Tyr444, FAD, and Tyr407 form an aromatic cage, which determines the final orientation of the inhibitors and hence their stabilization and activity. This proves that the effective complementary binding groups for MAO-A are present in the 3-hydroxy-3-phenacyloxindole analogues. Furthermore, these inhibitors are stabilized by π – π stacking and hydrogen bonding (H-bond) interactions.

All compounds showed π – π interactions except compounds **9**, **10**, **12**, and **16**. A π – π interaction with Tyr407 was observed with compounds **11**, **13–15**, **20**, and **22–27**, and with Tyr444 for compounds **15**, **17**, **20**, **23**, **25**, and **26**. The binding of compound **18** is also stabilized by a π – σ interaction with Tyr407; the same is true for **24** with Phe208, and for **21** and **25** with FAD. All compounds showed one or more H-bond interaction except compound **23**. Thus, in most of the potent compounds, preferably π – π , π – σ hydrophobic, and H-bond interactions were found to be responsible for mediating the inhibitory activity against MAO-A.

Examination of one of the best-ranked docking solutions of lead MAO-A inhibitor **18** (Figure 6C) revealed that the oxindole nucleus is located at the center of the cavity, while the phenacyl side chain extends toward the FAD cofactor, and the benzyl moiety is situated toward the opening of the MAO-A active site. From the molecular modeling studies, it was shown that **18** can access deep inside the cavity of MAO-A. The entire molecule appears to be entrapped by residues Tyr197, Asn181, Phe208, Ile325, Ile335, Phe352, Tyr407, Tyr444, and FAD. The C2 atom of the phenyl ring of the phenacyl side chain shows a π – σ interaction with FAD at an inter-plane distance of 3.89 Å. The molecule is also stabilized by several H-bond interactions. The carbonyl oxygen atom of the phenacyl side chain forms an H-bond with H5 and O4 of FAD. The oxygen atom of the 4-OH group on the phenyl ring of the phenacyl side chain is involved in H-bond interactions with the OH groups of Tyr444 at inter-plane distances of 2.41 and 2.38 Å, and with OH groups of Tyr197 at inter-plane distances of 3.19 and 2.24 Å, respectively. Moreover, the hydrogen atom of the 4-OH group on the phenyl ring of the phenacyl side chain also stabilizes the molecule by forming H-bond interactions with the oxygen atom of Asn181. As a whole, these interactions resulted in the rigidity of the ligand in the active site of MAO-A and hence demon-

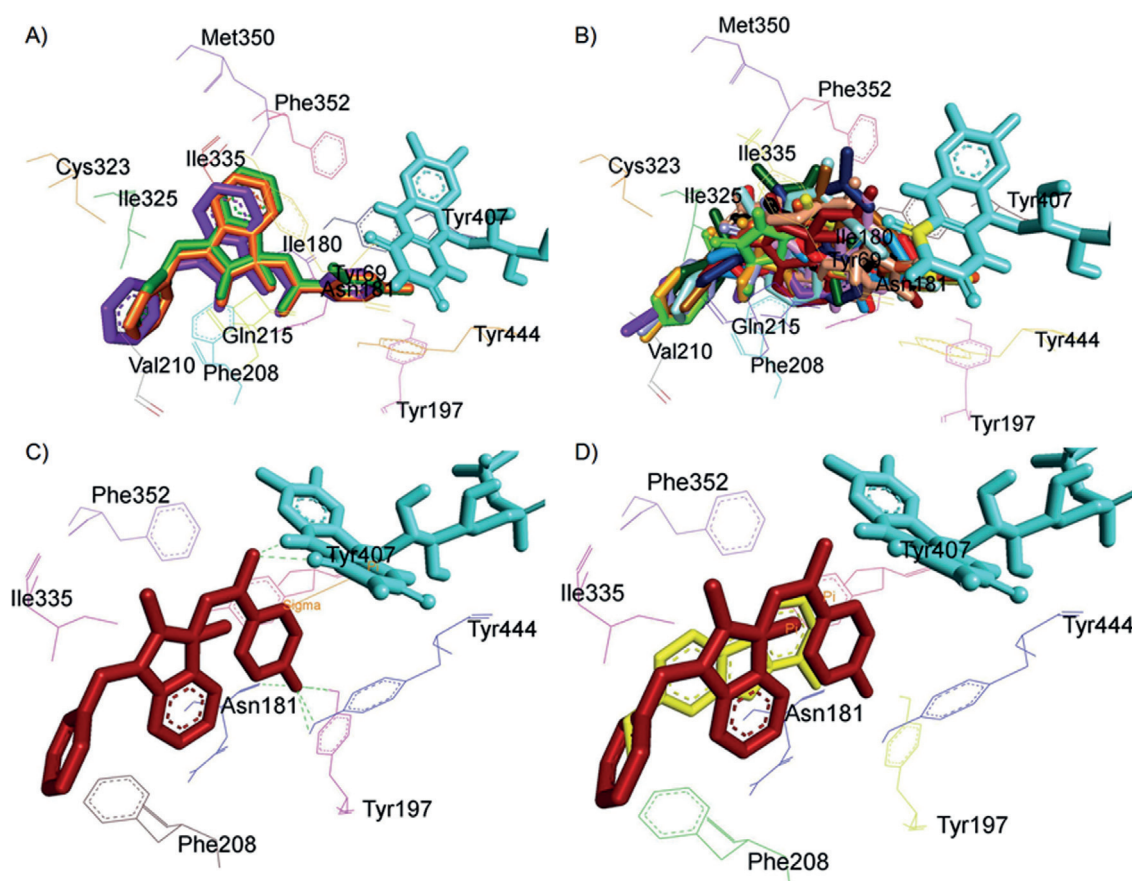


Figure 6. Superimposed MAO-A inhibitors docked into the active site of MAO-A. FAD is shown in cyan, and selected active site residues are highlighted. A) Compounds **15**, **17**, and **20** are displayed in violet, orange, and green, respectively. B) Compounds **9–14**, **16**, **18**, **19**, and **21–27** are shown in fluorescent green, violet, blue, crimson yellow, red, dark blue, brown, maroon, light blue, light pink, dark green, black, grey, yellow, orange, and light beige, respectively. C) Binding orientation of **18** (maroon) within the MAO-A active site, showing π - σ (orange lines) and H-bond (green dashes) interactions. D) Superimposed binding mode of **18** (maroon) in MAO-A originally docked with harmine (yellow).

strates the greater stability of the complex. The docked pose of **18** in the MAO-A active site superimposed with the pose of harmine (yellow) shows that both have a similar binding orientation (Figure 6D), which further supports our findings.

We also decided to consider both global minimum energy structures for the next docking simulations. These calculations were performed with hMAO-A and hMAO-B models, and the recognition of compound **18** was evaluated with the interaction energy parameter (Table 2).^[39] Compound **18** was found to undergo a more favorable interaction with hMAO-A than hMAO-B, which is in agreement with the experimental data, as reported in Table 2. An analysis of the interaction energy com-

ponents indicated a complete preference of compound **18** with respect to the A isoform in terms of both van der Waals and electrostatic contributions.

Pose analysis of MAO-B inhibitors

In contrast to MAO-A, the active site of MAO-B consists of two cavities: a 420 Å³ hydrophobic substrate cavity connected to an entrance cavity of 290 Å³.^[40] Compounds **14**, **15**, and **17** (Figure 7A) and compounds **9–13**, **16**, and **18–27** (Figure 7B) were observed to have a common binding mode within the active site cavity of MAO-B. Almost all the inhibitors are situated in the active site of MAO-B. Compounds **9–27** were found to be embedded in the space surrounded by residues Leu171, Cys172, and Tyr398 on one side, and by Ile198, Ile199, and Tyr435 on the other side, in addition to the aromatic residues Tyr60, Tyr326, and Phe343. Visual inspection revealed that the binding sites of inhibitors **9–27** are roughly similar to the binding sites of the standard MAO-B inhibitor, rasagiline. Furthermore, π - π stacking and H-bond interactions impart stability to these inhibitors.

Table 2. Interaction energies of compound **18** within hMAO-A and hMAO-B binding pockets.

	ΔE_{int} [kcal mol ⁻¹] ^[a]	vdW [kcal mol ⁻¹] ^[b]	EI [kcal mol ⁻¹] ^[c]
hMAO-A	-9.79	-9.63	-0.16
hMAO-B	-9.69	-9.59	-0.1

[a] Total interaction energy. [b] van der Waals contribution. [c] Electrostatic contribution.

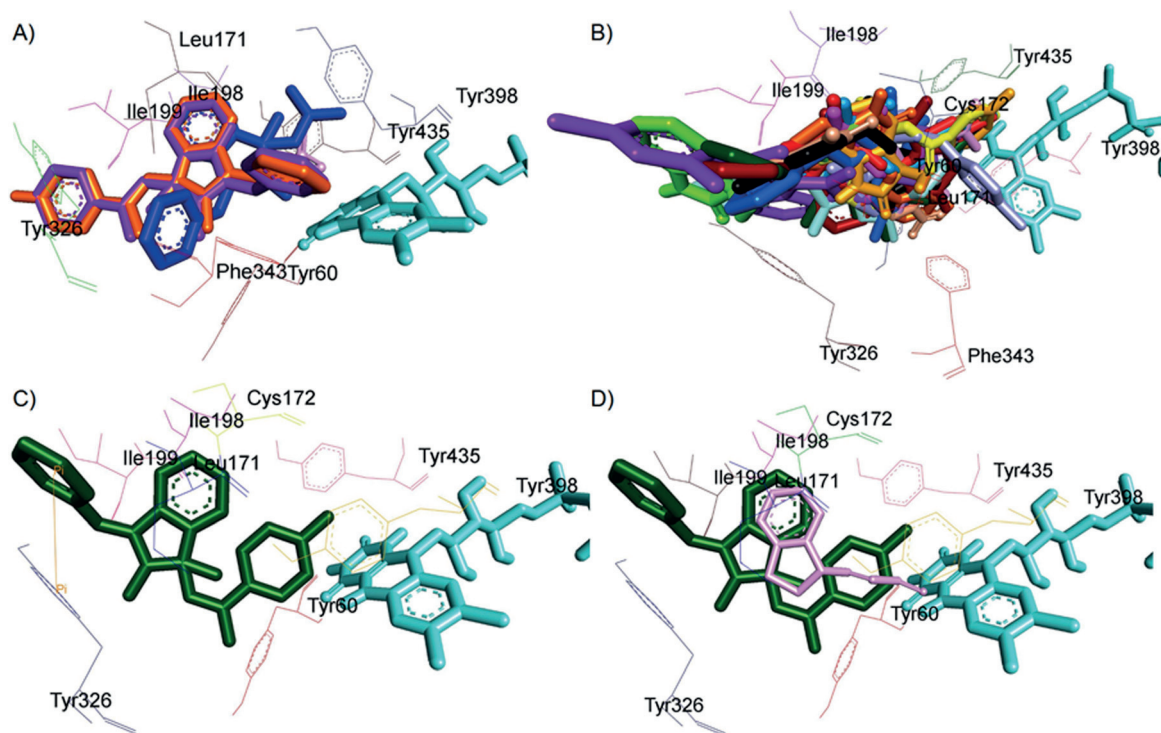


Figure 7. Superimposed MAO-B inhibitors docked into the active site of MAO-B. FAD is shown in cyan, and selected active site residues are highlighted. A) Compounds **14**, **15**, and **17** are displayed in dark blue, violet, and orange, respectively. B) Compounds **9–13**, **16**, and **18–27** are shown in fluorescent green, dark pink, blue, crimson yellow, red, dark green, maroon, light blue, violet, light pink, dark blue, black, grey, yellow, orange, and light beige, respectively. C) Binding orientation of **16** (dark green) within the MAO-B active site, showing π - π interactions (orange lines). D) Superimposed binding mode of **16** (dark green) in MAO-B originally docked with rasagiline (pink).

All compounds showed π - π interactions except compounds **9**, **22**, **26**, and **27**; π - π interactions with residue Tyr326 are observed with compounds **16** and **19**, and with Tyr398 for compounds **10–13**, **20**, and **23–25**. Moreover, compounds **15** and **17** were found to have π - π interactions with Phe343; likewise compounds **10–13**, **24**, and **25** with Tyr435. Compounds **18** and **24** are stabilized by a π - σ interaction with Tyr326; likewise compounds **11** and **23** with FAD, and compound **23** with Ile199. In addition, H-bond interactions were observed with Tyr435 for compounds **14**, **18**, **21**, **22** and **24**; with FAD for **14**, **18**, **21**, **26**, and **27**; with Cys172 for **10**, **11**, **13**, **18**, **22**, and **26**; with Tyr188 for **12** and **21**; with Tyr326 and Pro102 for **9**; with Gln206 for **10**, **11**, **13**, **23**, and **26**; with Phe168 for **27**; with Ile198 for **10**, **11**, **13**, **25**, **26**, and **27**; with Tyr398 for **12** and **25**; and with Leu171 for **12**. However, compounds **15–17**, **19**, and **20** lack H-bond interactions. Thus, in most of the potent compounds, preferably π - π and H-bond interactions were found to be responsible for mediating the inhibitory activity against MAO-B. Good van der Waals and electrostatic interactions with Pro102, Ile316, and Phe343 were also observed for all the docked molecules.

Inspection of the virtual complex between the lead MAO-B inhibitor **16** and MAO-B reveals that, in the substrate cavity, the oxindole ring is oriented with the *N*-benzyl moiety directed toward the entrance cavity and the 3-phenacyl side chain pointing toward the FAD cofactor (Figure 7C). This suggests that the whole molecule traverses both cavities. The entire

molecule is stabilized in both the cavities surrounded by residues Leu171, Cys172, Ile198, Ile199, and Tyr326 toward the entrance cavity space, and residues Tyr60, Tyr398, and Tyr435 frame the aromatic cage in the substrate cavity. The binding is further stabilized by various π - π interactions, one of which was observed between Tyr326 and the *N*-benzyl ring with an inter-plane distance of ~ 4.64 Å. Of importance is the observation that no H-bond interactions were found to be involved in displaying inhibitors activity toward MAO-B.

An overall analysis of the interactions of all inhibitors **9–27** with the anchoring residues present in the active site of MAO-B lead to the following observations: 1) The most potent compounds lack H-bond interactions (compounds **15–17**, **19**, and **20**). 2) π - π interactions were found to play an important role in mediating activity against MAO-B (all compounds except **9**, **22**, **26**, and **27**). 3) In addition to the oxindole skeleton, another hydrophobic aryl ring with electronegative substituents such as bromo, chloro, and fluoro groups, is crucial for their effective binding and stabilization in the active site cavity of MAO-B.

The dissimilarity between the experimental and computational results is due to variation in the sources of MAO-A and MAO-B isozymes. Therefore, exact experimental values were not expected from the computational work. This difference may also arise from the approximations and simplifications made during the computation process; for example, no explicit water molecules were considered during docking simulations.

Furthermore, AutoDock 4.2 uses an empirical scoring function for free energy calculations. Considering all these factors, a very reasonable prediction of IC_{50} values, inhibition constants (K_i values), and binding energies was obtained.

Conclusions

In this study, we designed and synthesized a new series of 3-hydroxy-3-phenacyloxindole analogues **9–27**. Interestingly, evaluation of the MAO-A and MAO-B inhibitory activities of these compounds revealed some highly potent and selective MAO-A inhibitors. The most active compound, 1-benzyl-3-hydroxy-3-(4'-hydroxyphenacyl)oxindole (**18**), possessing a hydroxy group at the *para* position of the 3-phenacyl ring, showed strong inhibitory activity against MAO-A (IC_{50} : 0.009 μ M) and has a selectivity index (SI) of 60.44 followed by **16** (IC_{50} : 0.013 μ M, SI: 8.54) and **20** (IC_{50} : 0.018 μ M, SI: 37.61), both of which have a bromo substituent in place of a hydroxy group. Furthermore, kinetic studies suggest that these compounds exhibit a competitive mode of enzyme inhibition. The *N*-benzylisatin-based 3-hydroxy-3-phenacyloxindole analogues were found to be more potent than *N*-unsubstituted isatin and 5-bromoisatin-based analogues. SAR studies revealed several structural factors important for the potency and selectivity of the designed analogues. First are multiple hydroxylations, one of which should be the hydroxylation at C3 of isatin in addition to hydroxylation at the *para* position of the 3-phenacyl ring. Second, bromination at the *para* position of the 3-phenacyl side chain is also important for MAO-A potency and selectivity, apart from the hydroxy group. Computational studies guided by an established docking protocol yielded a good correlation between the theoretical and experimental inhibitory data. Docking data and binding pose analysis of docked conformations revealed the importance of π - π and H-bond interactions for the effective stabilization of virtual inhibitor-MAO-A complexes. Furthermore, the binding orientation adopted by the oxindole moiety appears to be unimportant for modulating MAO-A inhibitory activity, because it assumes an opposite orientation between the two most active MAO-A inhibitors, compounds **18** and **20**. Besides these, the high MAO-A selectivity of 3-hydroxy-3-phenacyloxindole analogues could be ascribed to their molecular shape, enabling a better accommodation into the MAO-A binding site, which is wider and less flat than that of MAO-B.^[6,40]

These results provide a better understanding of the molecular fragments that are essential to maintain and/or improve MAO inhibitory activity and selectivity. These findings encourage us to continue our efforts toward optimization of the activity profile of this important scaffold in designing selective MAO inhibitors for the potential treatment of behavior- and age-related disorders associated with MAO activity.

Experimental Section

Chemistry

Unless otherwise specified, all starting materials and solvents were of commercial quality of laboratory grade purchased from Sigma-Aldrich and Merck and were used without purification. Melting points (mp) were determined in open capillary tubes on a Sonar melting point apparatus and are uncorrected. All intermediates and final compounds were characterized by IR, 1H NMR, ^{13}C NMR, and FAB-MS analyses. IR spectra were recorded on a Shimadzu FT-IR 8400S infrared spectrophotometer using KBr pellets. 1H and ^{13}C NMR spectra were recorded on a Jeol AL300 FT-NMR spectrometer at frequencies of 300 and 75 MHz, respectively. All NMR measurements were conducted in $[D_6]DMSO$. Chemical shifts (δ) are reported in parts per million (ppm) downfield from the signal of tetramethylsilane added to the deuterated solvent. Spin multiplicities are given as s (singlet), d (doublet), t (triplet), or m (multiplet). Mass spectra were recorded on a Thermo LCQ Advantage Max ion trap mass spectrometer. Elemental analyses (C, H, and N) were undertaken with an Exeter Analytical Inc. Model CE-440 CHN analyzer, and the observed values were within $\pm 0.4\%$ of calculated values.

Intermediates

General procedure for the synthesis of *N*-benzylisatin **7:** To a solution of isatin (0.0029 mol) in DMF (10 mL) containing potassium carbonate (0.007 mol), benzyl chloride (0.0029 mol) was added slowly with simultaneous stirring. The mixture was then heated on a water bath for ~ 4 h. The contents of the flask were then poured into cold water (50 mL), and the amorphous precipitate formed was filtered, dried, and recrystallized from acetonitrile to produce crystalline *N*-benzylisatin.^[35]

***N*-benzylisatin **7**:** Yield: 79.88%; mp: 112–116 $^{\circ}C$; IR (KBr): $\tilde{\nu}$ = 3454.62 ($3^{\circ}N$ str), 3030.27 (C–H arom str), 1734.06 (2 C=O str), 1612.54 (3 C=O str), 1467.88 (CH_2 bend), 1309.71 cm^{-1} (C–N str); 1H NMR (300 MHz, $[D_6]DMSO$): δ = 4.48 (s, 2H, Ar- CH_2), 7.19 (dd, J = 7.1, 2.2 Hz, 1H, ArC–H), 7.23 (dd, J = 7.3, 2.4 Hz 2H, ArC–H), 7.27 (d, J = 6.2 Hz, 2H, ArC–H), 7.32 (dd, J = 7.4, 2.3 Hz, 1H, oxindole C–H), 7.84 (dd, J = 7.6, 3.2 Hz, 1H, oxindole C–H), 7.85 (d, J = 7.6 Hz, 1H, oxindole C–H), 8.13 ppm (d, J = 2.6 Hz, 1H, oxindole C–H); ^{13}C NMR ($[D_6]DMSO$): δ = 43.29 (Ar- CH_2), 115.35 (oxindole C-3a), 123.72 (oxindole C-7), 124.68 (oxindole C-5), 125.81 (C'-4), 126.58 (C'-2, C'-6), 128.98 (C'-3, C'-5), 130.42 (oxindole C-4), 136.23 (oxindole C-6), 143.37 (C'-1), 145.67 (oxindole C-7a), 165.21 (oxindole C-2), 178.54 ppm (oxindole C-3).

General procedure for the synthesis of 5-bromoisatin **8:** To a solution of isatin (0.1 mol) in glacial acetic acid at $0^{\circ}C$ in a conical flask, bromine solution was added from the burette, until the loss of all color. The reaction mixture was then allowed to stand for 10–15 min and then poured into ice-cold water. The orange-colored precipitate was separated, filtered, and recrystallized from glacial acetic acid.^[36]

5-bromoisatin **8:** Yield: 89.43%; mp: 224–228 $^{\circ}C$; IR (KBr): $\tilde{\nu}$ = 3205.80 (N–H str), 2996.55 (arom C–H str), 1755.28 (2 C=O str), 1710.92 (3 C=O str), 1282.71 (C–N str), 886.52 (C–Br str), 464.86 cm^{-1} (C–Br str); 1H NMR (300 MHz, $[D_6]DMSO$): δ = 7.43 (d, J = 6.8 Hz, 1H, oxindole C–H), 7.58 (d, J = 7.1 Hz, 1H, oxindole C–H), 8.01 (s, 1H, oxindole C–H), 7.93 ppm (s, 1H, oxindole N–H); ^{13}C NMR ($[D_6]DMSO$): δ = 121.52 (oxindole C-3a), 123.27 (oxindole C-5), 125.78 (oxindole C-7), 132.15 (oxindole C-4), 136.32 (oxindole C-6), 145.23 (oxindole C-7a), 160.37 (oxindole C-2), 175.28 ppm (oxindole C-3).

Final products

General procedure for the synthesis of 3-hydroxy-3-phenacyloxindole analogues of isatin 9–13: Isatin (0.005 mol) and an equimolecular amount of unsubstituted or 4-substituted acetophenone (0.005 mol) were dissolved in absolute ethanol (10–12 mL) and diethylamine (10–15 drops) was added. The mixture was heated at reflux on a steam bath for 30 min. After standing for 5–7 days at room temperature, the products were collected by filtration, dried, and recrystallized from 95% ethanol.^[25–27]

3-hydroxy-3-phenacyloxindole 9: Yield: 42.67%; mp: 166–168 °C; IR (KBr): $\tilde{\nu}$ = 3306.10 (O–H str), 3254.02 (N–H str), 3097.78 (arom C–H str), 2914.54 (CH₂ str), 1712.85 (2 C=O str), 1681.98 (C=O str), 1597.11 (C=C str), 1477.52 cm⁻¹ (CH₂ bend); ¹H NMR (300 MHz, [D₆]DMSO): δ = 1.17 (s, 1H, CH₂), 1.19 (s, 1H, CH₂), 4.23 (s, 1H, O–H), 6.03 (dd, *J* = 7.2, 2.1 Hz, 1H, oxindole C–H), 6.77 (d, *J* = 6.5 Hz, 1H, oxindole C–H), 6.77 (dd, *J* = 7.3, 2.4 Hz, 1H, oxindole C–H), 6.80 (d, *J* = 6.5 Hz, 1H, oxindole C–H), 7.34 (dd, *J* = 7.8, 2.9 Hz, 2H, Ar'C–H), 7.47 (dd, *J* = 8.1, 3.3 Hz, 1H, Ar'C–H), 7.75 (d, *J* = 7.5 Hz, 2H, Ar'C–H), 7.85 ppm (s, 1H, oxindole N–H); ¹³C NMR ([D₆]DMSO): δ = 64.29 (–CH₂), 79.60 (oxindole C-3), 102.57 (oxindole C-7), 116.58 (oxindole C-5), 121.01 (oxindole C-6, oxindole C-3a), 122.38 (C'-3, C'-5), 126.04 (C'-2, C'-6), 131.89 (oxindole C-4), 153.38 (C'-4), 154.32 (C'-1), 154.85 (oxindole C-7a), 155.89 (oxindole C=O), 190.29 ppm (C=O); Anal. calcd for C₁₆H₁₃NO₃: C 71.90, H 4.90, N 5.24, found: C 71.95, H 4.93, N 5.20.

3-hydroxy-3-(4'-bromophenacyl)oxindole 10: Yield: 23.81%; mp: 176–179 °C; IR (KBr): $\tilde{\nu}$ = 3371.68 (O–H str), 3200.01 (N–H str), 3061.13 (arom C–H str), 2983.98 (CH₂ str), 1701.27 (2 C=O str), 1687.77 (C=O str), 1583.61 (C=C str), 1469.81 (CH₂ bend), 657.75 cm⁻¹ (C–Br str); ¹H NMR (300 MHz, [D₆]DMSO): δ = 4.20 (s, 1H, O–H), 3.06 (s, 1H, CH₂), 3.25 (s, 1H, CH₂), 6.59 (dd, *J* = 7.3, 2.2 Hz, 1H, oxindole C–H), 7.17 (d, *J* = 6.5 Hz, 1H, oxindole C–H), 7.21 (dd, *J* = 7.7, 2.5 Hz, 1H, oxindole C–H), 7.39 (d, *J* = 6.9 Hz, 1H, oxindole C–H), 7.49 (d, *J* = 7.1 Hz, 2H, Ar'C–H), 7.16 (d, *J* = 6.6 Hz, 2H, Ar'C–H), 7.69 ppm (s, 1H, oxindole N–H); ¹³C NMR ([D₆]DMSO): δ = 45.69 (–CH₂), 72.69 (oxindole C-3), 116.86 (C'-3, C'-5), 122.59 (oxindole C-7), 125.56 (oxindole C-5), 127.88 (oxindole C-6), 127.88 (oxindole C-3a), 128.72 (C'-4), 130.81 (oxindole C-4), 131.96 (C'-2, C'-6), 132.92 (C'-1), 143.28 (oxindole C-7a), 178.60 (oxindole C=O), 195.98 ppm (C=O); Anal. calcd for C₁₆H₁₂BrNO₃: C 55.51, H 3.49, N 4.05, found: C 55.58, H 3.46, N 4.09.

3-hydroxy-3-(4'-chlorophenacyl)oxindole 11: Yield: 59.86%; mp: 171–174 °C; IR (KBr): $\tilde{\nu}$ = 3375.54 (O–H str), 3196.15 (N–H str), 3059.20 (arom C–H str), 2902.96 (CH₂ str), 1699.34 (2 C=O str), 1683.91 (C=O str), 1587.47 (C=C str), 1471.74 (CH₂ bend), 750.33 cm⁻¹ (C–Cl str); ¹H NMR (300 MHz, [D₆]DMSO): δ = 3.50 (s, 1H, CH₂), 3.57 (s, 1H, CH₂), 4.05 (s, 1H, O–H), 6.86 (dd, *J* = 7.5, 2.4 Hz, 1H, oxindole C–H), 7.17 (d, *J* = 6.5 Hz, 1H, oxindole C–H), 7.24 (dd, *J* = 7.1, 1.9 Hz, 1H, oxindole C–H), 7.55 (d, *J* = 7.4 Hz, 1H, oxindole C–H), 7.26 (d, *J* = 6.8 Hz, 2H, Ar'C–H), 7.86 (d, *J* = 7.6 Hz, 2H, Ar'C–H), 7.89 ppm (s, 1H, oxindole N–H); ¹³C NMR ([D₆]DMSO): δ = 45.69 (–CH₂), 72.96 (oxindole C-3), 109.37 (oxindole C-7), 121.08 (oxindole C-5), 123.62 (oxindole C-3a), 128.74 (oxindole C-6), 128.91 (C'-3, C'-5), 129.82 (oxindole C-4), 131.53 (C'-2, C'-6), 134.85 (C'-1), 138.28 (C'-4), 142.79 (oxindole C-7a), 178.14 (oxindole C=O), 195.49 ppm (C=O); MS: *m/z* = 302.78 [*M*+1]⁺; Anal. calcd for C₁₆H₁₂ClNO₃: C 63.69, H 4.01, N 4.64, found: C 63.74, H 4.06, N 5.67.

3-hydroxy-3-(4'-fluorophenacyl)oxindole 12: Yield: 89.76%; mp: 204–206 °C; IR (KBr): $\tilde{\nu}$ = 3385.18 (O–H str), 3198.08 (N–H str), 3064.99 (arom C–H str), 2901.04 (CH₂ str), 1701.27 (2 C=O str), 1681.98 (C=O str), 1599.04 (C=C str), 1471.74 (CH₂ bend),

993.37 cm⁻¹ (C–F str); ¹H NMR (300 MHz, [D₆]DMSO): δ = 3.51 (s, 1H, CH₂), 3.57 (s, 1H, CH₂), 4.05 (s, 1H, O–H), 6.86 (dd, *J* = 7.5, 2.4 Hz, 1H, oxindole C–H), 7.17 (d, *J* = 6.5 Hz, 1H, oxindole C–H), 7.20 (dd, *J* = 7.7, 2.3 Hz, 1H, oxindole C–H), 7.46 (d, *J* = 7.2 Hz, 1H, oxindole C–H), 7.12 (s, 1H, oxindole N–H), 7.32 (d, *J* = 7.0 Hz, 2H, Ar'C–H), 7.95 ppm (d, *J* = 7.7 Hz, 2H, Ar'C–H); ¹³C NMR ([D₆]DMSO): δ = 45.66 (–CH₂), 72.97 (oxindole C-3), 115.78 (C'-3, C'-5), 121.06 (oxindole C-7), 123.58 (oxindole C-5), 128.87 (oxindole C-3a, oxindole C-6), 130.86 (oxindole C-4), 131.62 (C'-2, C'-6), 132.96 (C'-1), 142.84 (oxindole C-7a), 166.73 (C'-4), 178.19 (oxindole C=O), 195.04 ppm (C=O); Anal. calcd for C₁₆H₁₂FNO₃: C 67.36, H 4.24, N 4.91, found: C 67.42, H 4.26, N 4.95.

3-hydroxy-3-(2',4'-dibromophenacyl)oxindole 13: Yield: 32.35%; mp: 163–165 °C; IR (KBr): $\tilde{\nu}$ = 3368.54 (O–H str), 3210.14 (N–H str), 3095.85 (arom C–H str), 2970.48 (CH₂ str), 1732.13 (2 C=O str), 1685.84 (C=O str), 1581.68 (C=C str), 1465.95 (CH₂ bend), 648.10 cm⁻¹ (C–Br str); ¹H NMR (300 MHz, [D₆]DMSO): δ = 3.34 (s, 1H, CH₂), 3.90 (s, 1H, CH₂), 5.12 (s, 1H, O–H), 6.93 (dd, *J* = 7.6, 2.3 Hz, 1H, oxindole C–H), 7.25 (d, *J* = 6.7 Hz, 1H, oxindole C–H), 7.25 (dd, *J* = 7.8, 2.1 Hz, 1H, oxindole C–H), 7.71 (d, *J* = 7.3 Hz, 1H, oxindole C–H), 7.27 (d, *J* = 6.8 Hz, 2H, Ar'C–H), 7.74 (d, *J* = 7.5 Hz, 2H, Ar'C–H), 7.78 (s, 1H, Ar'C–H), 7.82 ppm (s, 1H, oxindole N–H); ¹³C NMR ([D₆]DMSO): δ = 60.43 (–CH₂), 63.50 (oxindole C-3), 111.01 (oxindole C-7), 119.16 (C'-2), 122.04 (oxindole C-5), 123.09 (oxindole C-3a), 123.09 (oxindole C-6), 128.67 (C'-4), 129.92 (oxindole C-4), 131.12 (C'-5), 132.22 (C'-6), 133.63 (C'-3), 143.99 (C'-1), 148.08 (oxindole C-7a), 170.64 (oxindole C=O), 190.36 ppm (C=O); Anal. calcd for C₁₆H₁₁Br₂NO₃: C 45.21, H 2.61, N 3.30, found: C 45.18, H 2.63, N 3.34.

General procedure for the synthesis of 3-hydroxy-3-phenacyloxindole analogues of N-benzylisatin 14–20: N-benzylisatin (0.005 mol) and an equimolecular amount of acetone or 4-substituted acetophenone (0.005 mol) were dissolved in absolute ethanol (10–12 mL), and diethylamine (10–15 drops) was added. After standing for 5–7 days at room temperature, the products were collected by filtration, dried and recrystallized from 95% ethanol.^[25–27]

1-benzyl-3-hydroxy-3-(2-oxopropyl)indolin-2-one 14: Yield: 53.0%; mp: 128–132 °C; IR (KBr): $\tilde{\nu}$ = 3313.82 (O–H str), 3091.99 (arom C–H str), 3063.06 (alkane C–H str), 1720.56 (2 C=O str), 1618.33 (C=O str), 1494.88 (C=C str), 1465.95 cm⁻¹ (CH₂ bend); ¹H NMR (300 MHz, [D₆]DMSO): δ = 2.17 (s, 3H, CH₃), 3.28 (s, 1H, CH₂), 3.76 (s, 1H, CH₂), 4.15 (s, 1H, O–H), 4.91 (s, 2H, Ar-CH₂), 7.11 (d, *J* = 6.3 Hz, 1H, oxindole C–H), 7.23 (dd, *J* = 6.9, 2.1 Hz, 1H, oxindole C–H), 7.33 (dd, *J* = 7.1, 1.9 Hz, 1H, oxindole C–H), 7.38 (d, *J* = 6.8 Hz, 1H, oxindole C–H), 7.49 (d, *J* = 8.2, 2.8 Hz, 2H, ArC–H), 7.59 (dd, *J* = 7.9, 2.2 Hz, 1H, ArC–H), 7.91 ppm (dd, *J* = 8.2, 2.8 Hz, 2H, ArC–H); ¹³C NMR ([D₆]DMSO): δ = 33.71 (–CH₃), 42.87 (Ar-CH₂), 45.58 (–CH₂), 72.30 (oxindole C-3), 118.68 (oxindole C-5), 120.07 (oxindole C-7), 123.81 (C'-4), 127.38 (C'-2, C'-6), 128.43 (oxindole C-3a), 129.94 (oxindole C-6), 130.94 (oxindole C-4), 131.78 (C'-3, C'-5), 141.59 (C'-1), 144.29 (oxindole C-7a), 176.79 (oxindole C=O), 195.34 ppm (C=O); Anal. calcd for C₁₈H₁₇NO₃: C 73.20, H 5.80, N 4.74, found: C 73.16, H 5.82, N 4.73.

1-benzyl-3-hydroxy-3-phenacyloxindole 15: Yield: 84.03%; mp: 170–174 °C; IR (KBr): $\tilde{\nu}$ = 3327.32 (O–H str), 3080.27 (arom C–H str), 1695.49 (2 C=O str), 1616.40 (C=O str), 1496.81 (C=C str), 1465.95 cm⁻¹ (CH₂ bend); ¹H NMR (300 MHz, [D₆]DMSO): δ = 3.69 (s, 1H, CH₂), 3.75 (s, 1H, CH₂), 4.22 (s, 1H, O–H), 4.91 (s, 2H, Ar-CH₂), 6.94 (d, *J* = 6.7 Hz, 2H, ArC–H), 7.13 (dd, *J* = 6.9, 2.0 Hz, 2H, ArC–H), 7.16 (dd, *J* = 7.0, 1.8 Hz, 1H, ArC–H), 6.77 (d, *J* = 6.5 Hz, 1H, oxindole C–H), 7.29 (dd, *J* = 7.3, 1.9 Hz, oxindole C–H), 7.35 (d, *J* =

6.8 Hz, 1H, oxindole C–H), 7.35 (dd, $J=7.5$, 2.3 Hz, 1H, oxindole C–H, 1H, oxindole C–H), 7.48 (dd, $J=7.9$, 2.9 Hz, 2H, ArC–H), 7.61 (dd, $J=8.3$, 3.2 Hz, 1H, ArC–H), 7.91 ppm (d, $J=7.6$ Hz, 2H, ArC–H); ^{13}C NMR ($[\text{D}_6]\text{DMSO}$): $\delta=42.71$ (Ar-CH₂), 45.87 (-CH₂), 72.73 (oxindole C-3), 108.86 (oxindole C-7), 121.89 (oxindole C-5), 123.31 (C'-4), 127.19 (C'-2, C'-6), 127.90 (oxindole C-3a), 127.90 (oxindole C-6), 128.39 (C'-3, C'-5), 128.67 (C''-3, C''-5), 128.89 (C''-2, C''-6), 131.05 (oxindole C-4), 133.45 (C''-4), 135.98 (C''-1), 136.39 (C'-1), 143.41 (oxindole C-7a), 176.77 (oxindole C=O), 196.44 ppm (C=O); Anal. calcd for C₂₃H₁₉NO₃: C 77.29, H 5.36, N 3.92, found: C 77.32, H 5.34, N 3.93.

1-benzyl-3-hydroxy-3-(4'-bromophenacyl)oxindole 16: Yield: 62.30%; mp: 228–230 °C; IR (KBr): $\tilde{\nu}=3462.34$ (O–H str), 3086.21 (arom C–H str), 1710.92 (2 C=O str), 1610.61 (C=O str), 1585.54 (C=C str), 1465.95 (CH₂ str), 698.25 cm⁻¹ (C–Br str); ^1H NMR (300 MHz, $[\text{D}_6]\text{DMSO}$): $\delta=3.48$ (s, 1H, CH₂), 3.65 (s, 1H, CH₂), 4.02 (s, 1H, O–H), 4.69 (s, 2H, Ar-CH₂), 6.81 (dd, $J=7.1$, 1.8 Hz, 1H, ArC–H), 6.91 (d, $J=6.7$ Hz, 2H, ArC–H), 6.71 (d, $J=6.5$ Hz, 1H, oxindole C–H), 7.25 (d, $J=6.9$ Hz, 1H, oxindole C–H), 7.35 (dd, $J=7.5$, 2.3 Hz, 1H, oxindole C–H), 7.47 (dd, $J=7.7$, 2.1 Hz, 1H, oxindole C–H), 7.49 (dd, $J=7.8$, 2.4 Hz, 2H, ArC–H), 7.68 (d, $J=7.3$ Hz, 2H, ArC–H), 7.90 ppm (d, $J=7.6$ Hz, 2H, ArC–H); ^{13}C NMR ($[\text{D}_6]\text{DMSO}$): $\delta=43.89$ (Ar-CH₂), 45.71 (-CH₂), 72.54 (oxindole C-3), 121.62 (oxindole C-7), 123.13 (C'-4), 124.28 (oxindole C-5), 125.46 (C''-4), 127.80 (oxindole C-3a), 127.86 (C''-3, C''-5), 127.94 (C'-2, C'-6), 128.13 (C'-3, C'-5), 128.16 (oxindole C-6), 128.97 (C''-2, C''-6), 130.14 (oxindole C-4), 135.55 (C''-1), 136.91 (C'-1), 143.00 (oxindole C-7a), 176.85 (oxindole C=O), 196.78 ppm (C=O); Anal. calcd for C₂₃H₁₈BrNO₃: C 63.32, H 4.16, N 3.21, found: C 63.30, H 4.17, N 3.22.

1-benzyl-3-hydroxy-3-(4'-fluorophenacyl)oxindole 17: Yield: 63.35%; mp: 164–168 °C; IR (KBr): $\tilde{\nu}=3352.39$ (O–H str), 3093.92 (arom C–H str), 1705.13 (2 C=O str), 1681.98 (C=O str), 1599.04 (C=C str), 1467.88 (CH₂ bend), 1003.02 cm⁻¹ (C–F str); ^1H NMR (300 MHz, $[\text{D}_6]\text{DMSO}$): $\delta=3.67$ (s, 1H, CH₂), 3.73 (s, 1H, CH₂), 4.19 (s, 1H, O–H), 4.89 (s, 2H, Ar-CH₂), 6.76 (d, $J=7.8$ Hz, 2H, ArC–H), 6.93 (d, $J=7.2$ Hz, 2H, ArC–H), 7.12 (dd, $J=6.9$, 1.9 Hz, 2H, ArC–H), 7.26 (dd, $J=7.2$, 1.8 Hz, 1H, ArC–H), 6.27 (d, $J=6.1$ Hz, 1H, oxindole C–H), 7.31 (dd, $J=7.1$, 1.8 Hz, 1H, oxindole C–H), 7.44 (d, $J=6.9$ Hz, 1H, oxindole C–H), 7.47 (dd, $J=7.7$, 2.1 Hz, 1H, oxindole C–H), 7.95 ppm (d, $J=7.7$ Hz, 1H, oxindole C–H, 2H, ArC–H); ^{13}C NMR ($[\text{D}_6]\text{DMSO}$): $\delta=42.72$ (Ar-CH₂), 45.83 (-CH₂), 72.75 (oxindole C-3), 108.89 (C''-3, C''-5), 115.83 (oxindole C-7), 121.91 (oxindole C-5), 123.36 (C'-4), 127.19 (C'-2, C'-6), 128.39 (oxindole C-3a), 128.94 (C'-3, C'-5), 130.99 (oxindole C-4), 131.07 (C''-2, C''-6), 132.80 (C''-1), 136.37 (C'-1), 143.36 (oxindole C-7a), 165.53 (C''-4), 176.72 (oxindole C=O), 195.07 ppm (C=O); Anal. calcd for C₂₃H₁₈FNO₃: C 73.59, H 4.83, N 3.73, found: C 73.63, H 4.82, N 3.71.

1-benzyl-3-hydroxy-3-(4'-hydroxyphenacyl)oxindole 18: Yield: 22.43%; mp: 120–122 °C; IR (KBr): $\tilde{\nu}=3325.39$ (O–H str), 3090.07 (arom C–H str), 1701.27 (2 C=O str), 1618.33 (C=O str), 1492.95 (C=C str), 1467.88 cm⁻¹ (CH₂ str); ^1H NMR ($[\text{D}_6]\text{DMSO}$): $\delta=3.24$ (s, 1H, CH₂), 3.64 (s, 1H, CH₂), 4.40 (s, 1H, O–H), 4.86 (s, 2H, Ar-CH₂), 5.09 (s, 1H, ArO–H), 6.73 (d, $J=7.4$ Hz, 2H, ArC–H), 6.99 (d, $J=6.9$ Hz, 2H, ArC–H), 6.87 (d, $J=6.3$ Hz, 1H, oxindole C–H), 7.00 (dd, $J=6.9$, 1.9 Hz, 1H, oxindole C–H), 7.38 (d, $J=6.8$ Hz, 1H, oxindole C–H), 7.69 (dd, $J=8.1$, 2.6 Hz, 1H, oxindole C–H), 7.26 (dd, $J=7.2$, 1.8 Hz, 2H, ArC–H), 7.73 (dd, $J=8.3$, 2.9 Hz, 1H, ArC–H), 7.92 ppm (d, $J=7.6$ Hz, 2H, ArC–H); ^{13}C NMR ($[\text{D}_6]\text{DMSO}$): $\delta=45.81$ (-CH₂), 48.96 (Ar-CH₂), 73.02 (oxindole C-3), 115.42 (C''-3, C''-5), 121.42 (oxindole C-7), 124.19 (oxindole C-5), 127.37 (oxindole C-3a), 127.47 (C'-4), 127.83 (oxindole C-6), 129.94 (C'-2, C'-6), 130.26 (C'-3, C'-5), 131.75 (C''-1), 133.26 (C''-2, C''-6), 134.65 (oxindole C-4), 141.11 (C'-1),

142.36 (oxindole C-7a), 162.24 (C''-4), 177.69 (oxindole C=O), 194.73 ppm (C=O); Anal. calcd for C₂₃H₁₉NO₄: C 73.98, H 5.13, N 3.75, found: C 74.01, H 5.11, N 3.74.

1-benzyl-3-hydroxy-3-(4'-nitrophenacyl)oxindole 19: Yield: 66.96%; mp: 136–140 °C; IR (KBr): $\tilde{\nu}=3460.41$ (O–H str), 3097.78 (arom C–H str), 1703.20 (2 C=O str), 1656.76 (C=O str), 1606.76 (C=C str), 1523.82, 1346.36 (Ar-NO₂ str), 1465.95 cm⁻¹ (CH₂ bend); ^1H NMR (300 MHz, $[\text{D}_6]\text{DMSO}$): $\delta=3.25$ (s, 1H, CH₂), 3.56 (s, 1H, CH₂), 4.23 (s, 1H, O–H), 4.86 (s, 2H, Ar-CH₂), 6.85 (d, $J=6.3$ Hz, 2H, ArC–H), 7.11 (dd, $J=6.8$, 1.7 Hz, 1H, ArC–H), 7.25 (dd, $J=7.2$, 1.9 Hz, 2H, ArC–H), 7.36 (d, $J=7.1$ Hz, 2H, ArC–H), 7.01 (d, $J=6.0$ Hz, 1H, oxindole C–H), 7.31 (d, $J=6.8$ Hz, 1H, oxindole C–H), 7.57 (dd, $J=7.8$, 2.6 Hz, 1H, oxindole C–H), 7.69 (dd, $J=8.1$, 3.1 Hz, 1H, oxindole C–H), 7.76 ppm (d, $J=7.5$ Hz, 2H, ArC–H); ^{13}C NMR ($[\text{D}_6]\text{DMSO}$): $\delta=43.27$ (Ar-CH₂), 44.11 (-CH₂), 73.68 (oxindole C-3), 122.82 (oxindole C-7), 123.07 (C''-3, C''-5), 125.35 (oxindole C-5), 126.13 (C'-4), 127.10 (C'-3, C'-5), 128.29 (oxindole C-3a), 128.44 (oxindole C-6), 128.91 (C'-2, C'-6), 131.58 (oxindole C-4), 132.30 (C''-2, C''-6), 135.32 (C'-1), 143.86 (C''-1), 144.74 (oxindole C-7a), 155.15 (C''-4), 169.54 (oxindole C=O), 190.41 ppm (C=O); Anal. calcd for C₂₃H₁₈N₂O₅: C 68.65, H 4.51, N 6.96, found: C 68.63, H 4.50, N 6.98.

1-benzyl-3-hydroxy-3-(2',4'-dibromophenacyl)oxindole 20: Yield: 91.36%; mp: 190–192 °C; IR (KBr): $\tilde{\nu}=3448.84$ (O–H str), 3092.87 (arom C–H str), 1726.35 (2 C=O str), 1681.98 (C=O str), 1612.54 (C=C str), 1469.81 (CH₂ str), 499.58, 565.16 cm⁻¹ (C–Br str); ^1H NMR (300 MHz, $[\text{D}_6]\text{DMSO}$): $\delta=3.32$ (s, 1H, CH₂), 3.86 (s, 1H, CH₂), 5.02 (s, 2H, Ar-CH₂), 5.29 (s, 1H, O–H), 6.96 (d, $J=6.4$ Hz, 2H, ArC–H), 7.06 (dd, $J=6.4$, 2.0 Hz, 2H, ArC–H), 7.27 (dd, $J=7.1$, 1.8 Hz, 1H, ArC–H), 6.88 (d, $J=6.5$ Hz, 1H, oxindole C–H), 7.32 (dd, $J=7.3$, 2.0 Hz, 1H, oxindole C–H), 7.36 (d, $J=6.9$ Hz, 1H, oxindole C–H), 7.36 (dd, $J=7.5$, 2.1 Hz, 1H, oxindole C–H, 1H, oxindole C–H), 7.37 (d, $J=7.2$ Hz, 1H, ArC–H), 7.76 (d, $J=7.5$ Hz, 1H, ArC–H), 7.83 ppm (s, 1H, ArC–H); ^{13}C NMR ($[\text{D}_6]\text{DMSO}$): $\delta=43.41$ (Ar-CH₂), 60.21 (-CH₂), 63.79 (oxindole C-3), 108.69 (C''-2), 109.71 (oxindole C-7), 110.48 (oxindole C-5), 118.80 (C'-4), 122.78 (C'-2, C'-6), 122.95 (oxindole C-3a), 122.95 (oxindole C-6), 127.23 (C'-3, C'-5), 127.60 (C''-4), 128.76 (oxindole C-4), 129.98 (C''-5), 131.11 (C''-6), 132.19 (C''-3), 133.59 (C''-1), 135.77 (C'-1), 144.35 (oxindole C-7a), 169.40 (oxindole C=O), 190.14 ppm (C=O); Anal. calcd for C₂₃H₁₇Br₂NO₃: C 53.62, H 3.33, N 2.72, found: C 53.65, H 3.32, N 2.73.

General procedure for the synthesis of 3-hydroxy-3-phenacyloxindole analogues of 5-bromoisatin 21–27: 5-Bromoisatin (0.003 mol) and an equimolecular amount of acetone or 4-substituted acetophenone (0.003 mol) were dissolved in absolute ethanol (10–12 mL), and diethylamine (10–15 drops) was added. The reaction mixture was heated at reflux on a steam bath for 30 min and allowed to stand for 7–10 days at room temperature, whereby the products formed were collected by filtration, dried and recrystallized from 95% ethanol.^[25–27]

5-bromo-3-hydroxy-3-(2-oxopropyl)indolin-2-one 21: Yield: 58.37%; mp: 184–188 °C; IR (KBr): $\tilde{\nu}=3581.93$ (O–H str), 3228.95 (N–H str), 3078.49 (arom C–H str), 2893.32 (alkane C–H str), 1701.27 (2 C=O str), 1618.33 (C=O str), 1479.45 (C=C str), 1448.59 (CH₂ bend), 840.99 cm⁻¹ (C–Br str); ^1H NMR (300 MHz, $[\text{D}_6]\text{DMSO}$): $\delta=2.18$ (s, 3H, CH₃), 2.91 (s, 1H, CH₂), 2.97 (s, 1H, CH₂), 4.02 (s, 1H, O–H), 7.75 (d, $J=7.5$ Hz, 1H, oxindole C–H), 7.26 (s, 1H, oxindole C–H), 7.85 (d, $J=7.7$ Hz, 1H, oxindole C–H), 7.98 ppm (s, 1H, oxindole N–H); ^{13}C NMR ($[\text{D}_6]\text{DMSO}$): $\delta=33.59$ (-CH₃), 44.99 (-CH₂), 79.64 (oxindole C-3), 121.51 (oxindole C-5), 125.00 (oxindole C-7), 128.84 (oxindole C-6), 131.00 (oxindole C-3a), 135.08 (oxindole C-4), 140.58 (oxindole C-7a), 175.78 (oxindole C=O), 190.97 ppm (C=O);

Anal. calcd for $C_{11}H_{10}BrNO_3$: C 46.50, H 3.55, N 4.93, found: C 46.53, H 3.57, N 4.91.

5-bromo-3-hydroxy-3-phenacyloxindole 22: Yield: 83.26%; mp: 192–196 °C; IR (KBr): $\tilde{\nu}$ = 3320.67 (O–H str), 3223.16 (N–H str), 3096.78 (arom C–H str), 2893.32 (alkane C–H str), 1708.99 (2 C=O str), 1683.91 (C=O str), 1618.33 (C=C str), 1448.59 (CH₂ bend), 842.92 cm⁻¹ (C–Br str); ¹H NMR (300 MHz, [D₆]DMSO): δ = 3.59 (s, 1H, CH₂), 3.65 (s, 1H, CH₂), 4.18 (s, 1H, O–H), 6.79 (dd, J = 6.6, 2.1 Hz, 2H, Ar'C–H), 7.35 (d, J = 6.8 Hz, 1H, oxindole C–H), 7.35 (s, 1H, oxindole C–H), 7.61 (d, J = 7.1 Hz, 1H, oxindole C–H), 7.52 (dd, J = 7.1, 1.9 Hz, 1H, Ar'C–H), 7.63 (d, J = 7.2 Hz, 2H, Ar'C–H), 7.89 ppm (s, 1H, oxindole N–H); ¹³C NMR ([D₆]DMSO): δ = 45.70 (–CH₂), 73.00 (oxindole C-3), 111.81 (oxindole C-5), 112.86 (oxindole C-7), 126.67 (C''-3, C''-5), 127.93 (C''-2, C''-6), 128.74 (oxindole C-3a), 131.49 (oxindole C-6), 133.54 (C''-4), 134.36 (oxindole C-4), 135.91 (C''-1), 142.32 (oxindole C-7a), 177.92 (oxindole C=O), 196.58 ppm (C=O); Anal. calcd for $C_{16}H_{12}BrNO_3$: C 55.51, H 3.49, N 4.05, found: C 55.47, H 3.51, N 3.99.

5-bromo-3-hydroxy-3-(4'-bromophenacyl)oxindole 23: Yield: 12.36%; mp: 159–161 °C; IR (KBr): $\tilde{\nu}$ = 3471.98 (O–H str), 3365.90 (N–H str), 3082.35 (arom C–H str), 2983.98 (CH₂ str), 1701.56 (2 C=O str), 1685.84 (C=O str), 1587.47 (C=C str), 1483.31 (CH₂ bend), 628.81, 588.31 cm⁻¹ (C–Br str); ¹H NMR (300 MHz, [D₆]DMSO): δ = 3.04 (s, 1H, CH₂), 3.42 (s, 1H, CH₂), 4.04 (s, 1H, O–H), 6.69 (d, J = 6.3 Hz, 1H, oxindole C–H), 7.47 (s, 1H, oxindole C–H), 7.56 (d, J = 7.1 Hz, 1H, oxindole C–H), 7.32 (d, J = 6.7 Hz, 2H, Ar'C–H), 7.97 (s, 1H, oxindole N–H), 7.98 ppm (d, J = 7.8 Hz, 2H, Ar'C–H); ¹³C NMR ([D₆]DMSO): δ = 48.50 (–CH₂), 70.32 (oxindole OH), 112.61 (oxindole C-5), 118.68 (oxindole C-7), 128.93 (C''-4), 130.12 (oxindole C-3a), 132.69 (C''-2, C''-6), 133.53 (C''-3, C''-5), 134.11 (oxindole C-6), 138.38 (C''-1), 140.46 (oxindole C-4), 142.02 (oxindole C-7a), 175.67 (oxindole C=O), 196.47 ppm (C=O); Anal. calcd for $C_{16}H_{11}Br_2NO_3$: C 45.21, H 2.61, N 3.30, found: C 45.26, H 2.58, N 3.26.

5-bromo-3-hydroxy-3-(4'-chlorophenacyl)oxindole 24: Yield: 19.71%; mp: 116–118 °C; IR (KBr): $\tilde{\nu}$ = 3363.97 (O–H str), 3275.24 (N–H str), 3080.42 (arom C–H str), 2982.05 (CH₂ str), 1703.62 (2 C=O str), 1687.77 (C=O str), 1587.47 (C=C str), 1477.52 (CH₂ bend), 817.85 (C–Cl str), 692.47 cm⁻¹ (C–Br str); ¹H NMR (300 MHz, [D₆]DMSO): δ = 2.01 (s, 1H, CH₂), 2.04 (s, 1H, CH₂), 4.23 (s, 1H, O–H), 7.37 (d, J = 6.8 Hz, 2H, Ar'C–H), 6.76 (d, J = 6.5 Hz, 1H, oxindole C–H), 7.74 (s, 1H, oxindole C–H), 7.57 (d, J = 7.0 Hz, 1H, oxindole C–H), 7.94 (d, J = 7.6 Hz, 2H, Ar'C–H), 7.96 ppm (s, 1H, oxindole N–H); ¹³C NMR ([D₆]DMSO): δ = 48.45 (–CH₂), 60.20 (oxindole OH), 102.14 (oxindole C-5), 118.78 (oxindole C-7), 124.12 (oxindole C-3a), 128.69 (C''-3, C''-5), 131.35 (C''-2, C''-6), 132.87 (C''-1), 138.39 (C''-4), 144.61 (oxindole C-6), 145.06 (oxindole C-4), 152.02 (oxindole C-7a), 165.71 (oxindole C=O), 194.61 ppm (C=O); MS: m/z = 381.88 [$M+1$]⁺; Anal. calcd for $C_{16}H_{11}BrClNO_3$: C 50.49, H 2.91, N 3.68, found: C 50.46, H 2.94, N 3.70.

5-bromo-3-hydroxy-3-(4'-fluorophenacyl)oxindole 25: Yield: 25.34%; mp: 156–159 °C; IR (KBr): $\tilde{\nu}$ = 3483.56 (O–H str), 3373.61 (N–H str), 3080.42 (arom C–H str), 2982.05 (CH₂ str), 1718.63 (2 C=O str), 1685.84 (C=O str), 1597.11 (C=C str), 1467.88 (CH₂ bend), 1031.95 (C–F str), 590.24 cm⁻¹ (C–Br str); ¹H NMR (300 MHz, [D₆]DMSO): δ = 3.28 (s, 1H, CH₂), 3.31 (s, 1H, CH₂), 4.25 (s, 1H, O–H), 6.77 (s, 1H, oxindole C–H), 6.79 (d, J = 6.5 Hz, 1H, oxindole C–H), 7.35 (d, J = 7.1 Hz, 1H, oxindole C–H), 6.73 (d, J = 6.3 Hz, 2H, Ar'C–H), 7.74 (d, J = 7.5 Hz, 2H, Ar'C–H), 7.96 ppm (s, 1H, oxindole N–H); ¹³C NMR ([D₆]DMSO): δ = 45.78 (–CH₂), 73.95 (oxindole OH), 111.60 (C''-3, C''-5), 112.19 (oxindole C-5), 115.742 (oxindole C-7), 126.54 (C''-2, C''-6), 127.43 (oxindole C-3a), 130.99 (C''-1), 131.43

(oxindole C-6), 134.46 (oxindole C-4), 142.63 (oxindole C-7a), 162.54 (C''-4), 177.37 (oxindole C=O), 194.74 ppm (C=O); Anal. calcd for $C_{16}H_{11}BrFNO_3$: C 52.77, H 3.04, N 3.85, found: C 52.81, H 3.07, N 3.90.

5-bromo-3-hydroxy-3-(4'-hydroxyphenacyl)oxindole 26: Yield: 42.81%; mp: 168–170 °C; IR (KBr): $\tilde{\nu}$ = 3368.54 (O–H str), 3210.14 (N–H str), 3095.85 (arom C–H str), 2970.48 (CH₂ str), 1732.13 (2 C=O str), 1685.84 (C=O str), 1581.68 (C=C str), 1465.95 (CH₂ bend), 648.10 cm⁻¹ (C–Br str); ¹H NMR (300 MHz, [D₆]DMSO): δ = 2.96 (s, 1H, Ar'-OH), 3.46 (s, 1H, CH₂), 3.52 (s, 1H, CH₂), 4.03 (s, 1H, O–H), 6.79 (d, J = 6.4 Hz, 2H, Ar'C–H), 7.30 (d, J = 6.9 Hz, 1H, oxindole C–H), 7.33 (d, J = 7.1 Hz, 1H, oxindole C–H), 7.45 (s, 1H, oxindole C–H), 7.74 (d, J = 7.5 Hz, 2H, Ar'C–H), 8.33 ppm (s, 1H, oxindole N–H); ¹³C NMR ([D₆]DMSO): δ = 45.18 (–CH₂), 73.05 (oxindole OH), 111.26 (C''-3, C''-5), 112.72 (oxindole C-5), 115.27 (oxindole C-7), 126.49 (C''-1), 127.34 (oxindole C-3a), 130.45 (C''-2, C''-6), 131.30 (oxindole C-6), 134.57 (oxindole C-4), 142.31 (oxindole C-7a), 162.75 (C''-4), 177.97 (oxindole C=O), 194.38 ppm (C=O); Anal. calcd for $C_{16}H_{12}BrNO_4$: C 53.06, H 3.34, N 3.87, found: C 53.02, H 3.36, N 3.90.

5-bromo-3-hydroxy-3-(4'-nitrophenacyl)oxindole 27: Yield: 13.52%; mp: charred at 188–190 °C; IR (KBr): $\tilde{\nu}$ = 3367.98 (O–H str), 3173.01 (N–H str), 3103.57 (arom C–H str), 2985.91 (CH₂ str), 1720.56 (2 C=O str), 1697.41 (C=O str), 1602.90 (C=C str), 1514.17 (CH₂ bend), 1464.02, 1346.36 (NO₂ str), 663.53 cm⁻¹ (C–Br str); ¹H NMR (300 MHz, [D₆]DMSO): δ = 3.26 (s, 1H, CH₂), 3.55 (s, 1H, CH₂), 4.07 (s, 1H, O–H), 7.28 (d, J = 7.0 Hz, 2H, Ar'C–H), 7.63 (d, J = 7.5 Hz, 1H, oxindole C–H), 7.56 (s, 1H, oxindole C–H), 7.21 (d, J = 6.6 Hz, 1H, oxindole C–H), 7.86 (d, J = 7.7 Hz, 2H, Ar'C–H), 7.98 ppm (s, 1H, oxindole N–H); ¹³C NMR ([D₆]DMSO): δ = 45.35 (–CH₂), 72.91 (oxindole OH), 120.86 (C''-3, C''-5), 121.08 (oxindole C-5), 123.07 (oxindole C-7), 128.88 (oxindole C-3a, oxindole C-6), 130.51 (oxindole C-4), 131.67 (C''-2, C''-6), 142.61 (C''-1), 143.58 (oxindole C-7a), 150.76 (C''-4), 178.17 (oxindole C=O), 195.80 ppm (C=O); Anal. calcd for $C_{16}H_{11}BrN_2O_5$: C 42.13, H 2.83, N 7.16, found: C 42.17, H 2.88, N 7.21.

Enzyme inhibition assays

Materials: 5-HT (serotonin) for MAO-A assay, benzylamine for MAO-B assay, and the reference inhibitors clorgyline (MAO-A) and selegiline (MAO-B) were purchased from Sigma-Aldrich. Tris-HCl, sodium phosphate and zinc sulfate were obtained from Merck and SD Fine.

Animal ethical approval: The Ethics Committee of Laboratory Animals at Banaras Hindu University, Varanasi (India), approved the animal experimentation reported herein. Albino Wistar rats weighing between 200 and 220 g were obtained from Central Animal House, Institute of Medical Sciences, Banaras Hindu University (Registration No. Dean/12-13/CAEC/23).

Isolation of rat brain mitochondria:^[41] Rat brain mitochondria were used as a source of the two MAO isoforms. All operations were carried out at 4 °C. Male and female adult Wistar rats weighing 200–220 g were decapitated. All brains were rapidly removed and homogenized with a Potter-Elvehjem homogenizer in cold 0.32 M sucrose and 50 mM Tris-HCl, pH 8.2 (10:1, v/w). The homogenate was centrifuged twice at 1000 g for 5 min at 4 °C. The resulting supernatant was centrifuged at 20000 g for 20 min. The mitochondrial pellet obtained was suspended in 100 mM sodium phosphate buffer, pH 7.4 (4:1, v/w), fractionated in plastic vials to 500 μ L samples and stored at –80 °C. Before use, mitochondria were diluted

with 100 mM sodium phosphate buffer to give a working solution of 0.84 mg protein per mL.

In vitro MAO inhibition assays: Experiments were carried out under all suitable laboratory conditions. The final compounds **9–27** were evaluated for their in vitro MAO-A inhibitory activity according to a method reported by Sjoerdsma et al.^[42] for the metabolism of serotonin, and by the UV spectrophotometric method described by Udenfriend et al.,^[43] which was applied for the determination of serotonin. Inhibitory activity of MAO-B was measured using benzylamine as a substrate according to the procedure reported by Tabor et al.^[44] with necessary modifications. The rat mitochondrial protein content was determined according to Lowry et al.,^[45] with bovine serum albumin as the standard. The test compounds were dissolved in DMSO and added to the buffered incubation mixture such that the final DMSO concentration was 4%, which caused no MAO inhibition. Clorgyline, selegiline, and isatin were taken as reference inhibitors for the determination of MAO-A and MAO-B activity, respectively. An aliquot was made to contain a mixture of 55 μ L mitochondrial suspension (0.84 mg protein per mL), 90 μ L 50 mM Tris-HCl buffer, pH 8.2 and 30 μ L solubilizing solution (control or inhibitor solution at five different concentrations). The reaction was initiated by adding 25 μ L of serotonin (4 mM, substrate for MAO-A) for evaluation of MAO-A activity, and 25 μ L benzylamine (0.1 M, substrate for MAO-B) for the determination of MAO-B activity. The mixture was incubated at 37 °C for 30 min, and the reaction was stopped by the addition of 1 mL 3% ice-cold zinc sulfate solution. It was subsequently mixed by vortexing for 10 s and then centrifuged using a fixed-angle rotor at 3000 rpm for 15 min. The supernatant was taken up, and the absorbance was read at λ 280 nm (due to formation of 5-hydroxyindolacetic acid) for MAO-A estimation and at 250 nm (due to the formation of benzaldehyde) for MAO-B estimation. All assays were performed in duplicate and were repeated twice. Control experiments were carried out without inhibitor, and blanks were run without mitochondrial suspension.^[46]

Data analysis: IC₅₀ values were calculated with 95% confidence limits by using Prism GraphPad Software (version 5.0), from plots of inhibition percentages (calculated in relation to a sample of the enzyme treated under the same conditions without inhibitor) versus the logarithm of the inhibitor concentration.

Reversibility and irreversibility experiments: To determine whether the observed enzyme inhibition is reversible or irreversible, a time-dependent inhibition study was carried out with a representative MAO-A inhibitor, compound **18**. Reversibility tests were performed by using a slightly modified method described by Legoabe et al.^[37] Compound **18** was allowed to pre-incubate with the mitochondrial working solution (0.84 mg protein per mL) for various periods of time (0, 15, 30, 60 min) at 37 °C in Tris-HCl buffer (50 mM, pH 8.2). For this purpose, the concentration of compound **18** was equal to twofold the measured IC₅₀ value for the inhibition of MAO-A (18 nM). The reactions were subsequently diluted twofold by the addition of 4 mM serotonin to yield a final enzyme concentration of 0.41 mg mL⁻¹ and concentrations of compound **18** that are equal to the IC₅₀ values. The reactions were incubated at 37 °C for a further 15 min, and the residual enzyme activities were measured; from these, bar graphs were constructed. All measurements were carried out in triplicate and are expressed as the mean \pm SEM.

In silico studies

Platform: A computational approach through docking calculations was used to better understand the possible binding orientations of

the test inhibitors within the active sites of MAO-A and MAO-B. The molecular docking studies were carried out with PC-based machines running Windows 7 (x86) as operating system.

Software: The molecular modelling software included MGL tools 1.5.4 based AutoDock 4.2 (www.scripps.edu) which uses Python 2.7 language—Cygwin C:\ program (www.cygwin.com) and Python 2.5 (www.python.com). Discovery Studio Visualizer 3.1 (www.accelrys.com) was used for visualizing the docked molecules.

Protein preparation: The X-ray crystallographic structures of human MAO-A co-crystallized with harmine (PDB ID: 2Z5X, resolution = 2.20 Å)^[7] and human MAO-B co-crystallized with rasagiline (PDB ID: 1S2Q, resolution = 2.07 Å)^[47] were retrieved from the RCSB Protein Data Bank (www.rcsb.org/pdb). These models were selected based on the relatively high resolution of the crystallographic structures. Furthermore, in the complex between MAO-B and rasagiline, the side chain of Ile199 is rotated out of the normal conformation. This allows fusion of the entrance and substrate cavities which is a necessity for the binding of relatively bulky ligands that span both the entrance and substrate cavities.^[47] In contrast, the active site of MAO-A consists of a single cavity.

Coordinate file preparation: Computational studies were carried out on only one subunit of the MAO isozymes. The PDB files obtained from Protein Data Bank were edited, and the β -chain was removed together with the complexed inhibitor except FAD from the active site. All water molecules and all non-interacting ions were also removed. This refinement in the crystal structure of both isozymes was carried out with the help of Discovery Studio Visualizer. An extended PDB format, termed as a PDBQT file, was used for coordinate files which includes atomic partial charges. AutoDock Tools was used for creating PDBQT files from traditional PDB files.^[48]

Ligand preparation: The structures of the test ligand and standard ligand molecules were built with the aid of the MarvinSketch 5.6 module of ChemAxon tools (www.chemaxon.com) and optimized using "Prepare Ligands" in AutoDock 4.2 and saved in PDB format. The partial charges of the PDB files were further modified using the ADT package (version 1.4.6) so that the charges of the nonpolar hydrogen atoms were assigned to the atom to which the hydrogen is attached. The resulting files were saved as PDBQT files.^[38]

Docking methodology: The refined protein molecules (2Z5X for MAO-A and 1S2Q for MAO-B) were used, and the docking methodology was performed according to a previously reported protocol.^[49]

Acknowledgements

R.K.P.T. is thankful to the Indian Council of Medical Research, New Delhi for the award of a Senior Research Fellowship.

Keywords: 3-hydroxy-3-phenacyloxyindoles • inhibitors • isatin • molecular docking • monoamine oxidase

- [1] C. Binda, J. Wang, L. Pisani, C. Caccia, A. Carotti, P. Salvati, D. E. Edmondson, A. Mattevi, *J. Med. Chem.* **2007**, *50*, 5848–5852.
- [2] L. Novaroli, A. Daina, E. Favre, J. Bravo, A. Carotti, F. Leonetti, M. Catto, P. Carrupt, M. Reist, *J. Med. Chem.* **2006**, *49*, 6264–6272.
- [3] P. Dostert, M. Strolin Benedetti, M. Jafre in *Monoamine Oxidase: Basic and Clinical Frontiers* (Eds.: K. Kamijo, E. Usdin, T. Nagausu), Excerpta Medica, Amsterdam, **1982**, pp. 197–208.

- [4] T. P. Singer in *Chemistry and Biochemistry of Flavoenzymes II* (Ed.: F. Muller), CRC Press, London, **1991**, pp. 437–470.
- [5] J. Ma, M. Yoshimura, E. Yamashita, A. Nakagawa, A. Ito, T. Tsukihara, *J. Mol. Biol.* **2004**, *338*, 103–114.
- [6] L. De Colibus, M. Li, C. Binda, A. Lustig, D. E. Edmondson, A. Mattevi, *Proc. Natl. Acad. Sci. USA* **2005**, *102*, 12684–12689.
- [7] S. Y. Son, J. Ma, Y. Kondou, M. Yoshimura, E. Yamashita, T. Tsukihara, *Proc. Natl. Acad. Sci. USA* **2008**, *105*, 5739–5744.
- [8] C. Binda, M. Li, F. Hubalek, N. Restelli, D. E. Edmondson, A. Mattevi, *Proc. Natl. Acad. Sci. USA* **2003**, *100*, 9750–9755.
- [9] M. Yamada, H. Yasuhara, *Neurotoxicology* **2004**, *25*, 215–221.
- [10] M. V. Rudorfer, W. Z. Potter, *Drugs* **1989**, *37*, 713–738.
- [11] S. Pahlagen, E. Heinonen, J. Hagglund, T. Kaugesaar, O. Maki-Ikola, R. Palm, *Neurology* **2006**, *66*, 1200–1206.
- [12] D. R. Guay, *Am. J. Geriatr. Pharmacother.* **2006**, *4*, 330–346.
- [13] P. Riederer, W. Danielczyk, E. Grunblatt, *Neurotoxicology* **2004**, *25*, 271–277.
- [14] M. B. H. Youdim, M. Fridkin, H. Zheng, *J. Neural Transm.* **2004**, *111*, 1455–1471.
- [15] A. M. Cesura, A. Pletscher, *Prog. Drug Res.* **1992**, *38*, 171–297.
- [16] L. Santana, H. Gonzalez-Diaz, E. Quezada, E. Uriarte, M. Yanez, D. Vina, F. Orallo, *J. Med. Chem.* **2008**, *51*, 6740–6751.
- [17] S. Carradori, J. P. Petzer, *Expert Opin. Ther. Pat.* **2015**, *25*, 91–110.
- [18] A. Bolasco, R. Fioravanti, S. Carradori, *Expert Opin. Ther. Pat.* **2005**, *15*, 1763–1782.
- [19] A. Bolasco, S. Carradori, R. Fioravanti, *Expert Opin. Ther. Pat.* **2010**, *20*, 909–939.
- [20] S. Carradori, D. Secci, A. Bolasco, P. Chimenti, M. D'Ascenzo, *Expert Opin. Ther. Pat.* **2012**, *22*, 759–801.
- [21] F. Hubalek, C. Binda, A. Khalil, M. Li, A. Mattevi, N. Castagnoli, Jr., D. E. Edmondson, *J. Biol. Chem.* **2005**, *280*, 15761–15766.
- [22] V. Glover, J. Halket, P. J. Watkins, A. Clow, B. L. Goodwin, M. Sandler, *J. Neurochem.* **1988**, *51*, 656–659.
- [23] S. N. Pandeya, S. Smitha, M. Jyoti, S. K. Sridhar, *Acta Pharm.* **2005**, *55*, 27–46 and references therein.
- [24] V. Glover, S. K. Bhattacharya, M. Sandler, *Indian J. Exp. Biol.* **1991**, *29*, 1–5.
- [25] a) F. D. Popp, R. Parson, B. E. Donigan, *J. Pharm. Sci.* **1980**, *69*, 1235–1237; b) F. D. Popp, R. Parson, B. E. Donigan, *J. Heterocycl. Chem.* **1980**, *17*, 1329–1330.
- [26] a) F. D. Popp, H. Pajouhesh, *J. Pharm. Sci.* **1982**, *71*, 1052–1054; b) F. D. Popp, *J. Heterocycl. Chem.* **1982**, *19*, 589–592.
- [27] H. Pajouhesh, R. Parson, F. D. Popp, *J. Pharm. Sci.* **1983**, *72*, 318–321.
- [28] B. Strydom, S. F. Malan, N. Castagnoli, Jr., J. J. Bergh, J. P. Petzer, *Bioorg. Med. Chem.* **2010**, *18*, 1018–1028.
- [29] L. H. Mu, B. Wang, H. Y. Ren, P. Liu, D. H. Guo, F. M. Wang, L. Bai, Y. S. Guo, *Bioorg. Med. Chem. Lett.* **2012**, *22*, 3343–3348.
- [30] J. Wouters, *Curr. Med. Chem.* **1998**, *5*, 137–162.
- [31] M. J. Matos, D. Vina, C. Picciau, F. Orallo, L. Santana, E. Uriarte, *Bioorg. Med. Chem. Lett.* **2009**, *19*, 5053–5055.
- [32] M. B. H. Youdim, A. Gross, J. P. M. Finberg, *British J. of Pharmacol.* **2001**, *132*, 500–506.
- [33] D. J. McKenna, G. H. Towers, F. Abbott, *J. Ethnopharmacol.* **1984**, *10*, 195–223.
- [34] J. Gerardy, *Prog. Neuro-Psychopharmacol. Biol. Psychiatry* **1994**, *18*, 793–802.
- [35] J. F. M. Da Silva, S. J. Garden, C. Da, A. Pinto, *J. Braz. Chem. Soc.* **2001**, *12*, 273–324.
- [36] S. N. Pandeya, A. S. Raja, J. P. Stables, *J. Pharm. Pharm. Sci.* **2002**, *5*, 266–271.
- [37] L. J. Legoabe, A. Petzer, J. P. Petzer, *Eur. J. Med. Chem.* **2012**, *49*, 343–353.
- [38] D. S. Goodsell, G. M. Morris, A. J. Olson, *J. Mol. Recognit.* **1996**, *9*, 1–5.
- [39] F. Chimenti, A. Bolasco, D. Secci, P. Chimenti, A. Granese, S. Carradori, M. Yáñez, F. Orallo, F. Ortuso, S. Alcaro, *Bioorg. Med. Chem.* **2010**, *18*, 5715–5723.
- [40] C. Binda, P. Newton-Vinson, F. Hubalek, D. E. Edmondson, A. Mattevi, *Nat. Struct. Biol.* **2002**, *9*, 22–26.
- [41] P. R. Reinhart, W. M. Taylor, F. L. Bygrave, *Biochem. J.* **1982**, *204*, 731–735.
- [42] A. Sjoerdsma, T. E. Smith, T. D. Stevenson, S. Udenfriend, *Proc. Soc. Exp. Biol. Med.* **1955**, *89*, 36–38.
- [43] S. Udenfriend, H. Weissbach, C. T. Clark, *J. Biol. Chem.* **1955**, *215*, 337–344.
- [44] C. Tabor, W. H. Tabor, S. M. Rosenthal, *J. Biol. Chem.* **1954**, *208*, 645–661.
- [45] O. H. Lowry, N. J. Rosebrough, A. L. Farr, R. T. Randall, *J. Biol. Chem.* **1951**, *193*, 265–275.
- [46] H. Park, M.-U. Choi, *Korean J. Biochem.* **1983**, *16*, 189–198.
- [47] C. Binda, F. Hubalek, M. Li, Y. Herzig, J. Sterling, D. E. Edmondson, *J. Med. Chem.* **2004**, *47*, 1767–1774.
- [48] A. Madeswaran, M. Umamaheswari, K. Asokkumar, T. Sivashanmugam, V. Subhadradevi, P. Jagannath, *J. Comput. J. Comput. Methods Mol. Des.* **2011**, *1*, 65–72.
- [49] R. K. P. Tripathi, O. Goshain, S. R. Ayyannan, *ChemMedChem* **2013**, *8*, 462–474.

Received: September 27, 2015

Revised: November 1, 2015

Published online on November 23, 2015